A Novel Network Profiling Analysis Reveals System Changes in Epithelial-Mesenchymal Transition

Teppei Shimamura[1]*, Seiya Imoto[1], Yukako Shimada[2], Yasuyuki Hosono[2], Atsushi Niida[1], Masao Nagasaki[1], Rui Yamaguchi[1], Takashi Takahashi[2], Satoru Miyano[1]

[1] Human Genome Center, Institute of Medical Science, University of Tokyo, Minato-ku, Tokyo, Japan, [2] Nagoya University Graduate School of Medicine, Showa-ku, Nagoya, Japan

Abstract

Patient-specific analysis of molecular networks is a promising strategy for making individual risk predictions and treatment decisions in cancer therapy. Although systems biology allows the gene network of a cell to be reconstructed from clinical gene expression data, traditional methods, such as Bayesian networks, only provide an averaged network for all samples. Therefore, these methods cannot reveal patient-specific differences in molecular networks during cancer progression. In this study, we developed a novel statistical method called NetworkProfiler, which infers patient-specific gene regulatory networks for a specific clinical characteristic, such as cancer progression, from gene expression data of cancer patients. We applied NetworkProfiler to microarray gene expression data from 762 cancer cell lines and extracted the system changes that were related to the epithelial-mesenchymal transition (EMT). Out of 1732 possible regulators of E-cadherin, a cell adhesion molecule that modulates the EMT, NetworkProfiler, identified 25 candidate regulators, of which about half have been experimentally verified in the literature. In addition, we used NetworkProfiler to predict EMT-dependent master regulators that enhanced cell adhesion, migration, invasion, and metastasis. In order to further evaluate the performance of NetworkProfiler, we selected Krueppel-like factor 5 (KLF5) from a list of the remaining candidate regulators of E-cadherin and conducted *in vitro* validation experiments. As a result, we found that knockdown of KLF5 by siRNA significantly decreased E-cadherin expression and induced morphological changes characteristic of EMT. In addition, *in vitro* experiments of a novel candidate EMT-related microRNA, miR-100, confirmed the involvement of miR-100 in several EMT-related aspects, which was consistent with the predictions obtained by NetworkProfiler.

Citation: Shimamura T, Imoto S, Shimada Y, Hosono Y, Niida A, et al. (2011) A Novel Network Profiling Analysis Reveals System Changes in Epithelial-Mesenchymal Transition. PLoS ONE 6(6): e20804. doi:10.1371/journal.pone.0020804

Editor: Eric J. Bernhard, National Cancer Institute, United States of America

Received November 2, 2010; **Accepted** May 13, 2011; **Published** June 7, 2011

Funding: This research was supported by "Research and Development of the Next-Generation Integrated Simulation of Living Matter" (a part of the Development and Use of the Next-Generation Supercomputer Project of MEXT) and "Integrative Systems Understanding of Cancer for Advanced Diagnosis, Therapy and Prevention" (Grant-in-Aid for Scientific Research on Innovative Areas from MEXT, Japan). The funders had no role in study design, data collection and analysis, decision to publish, or preparation of the manuscript.

Competing Interests: The authors have declared that no competing interests exist.

* E-mail: shima@ims.u-tokyo.ac.jp

Introduction

Currently, several large-scale omics projects, such as the National Cancer Institute's Cancer Genome Atlas (http://cancergenome.nih.gov/) and the Sanger Institute's Cancer Genome Project (http://www.sanger.ac.uk/genetics/CGP/), produce large amounts of data, including genomic, epigenomic, and transcriptomic information, about cancer patients or cell lines. Two challenges in omics are to construct and analyze patient-specific molecular networks to develop a comprehensive understanding of the molecular mechanisms of tumorigenesis and to identify molecules that are critical for tumor proliferation and progression [1]. If these challenges can be overcome, it may be possible to personalize cancer therapy, improve its efficacy, and reduce its toxicity and cost [2,3].

Systems biology integrates various types of omics data and computational tools to represent and analyze complex biological systems. For example, gene network estimation that is based on Bayesian networks or mutual information networks can reconstruct biological systems from gene expression data [4]. However, most traditional gene network estimation methods construct a static network by using gene expression data from different cellular conditions. As a result, these methods only produce an averaged network for all patients and cannot reveal patient-specific molecular mechanisms of cancer. In addition, it is very difficult to infer a patient-specific gene network from only a few gene expression profiles of the patient without making any assumptions about the network.

In this study, we developed a novel statistical method called NetworkProfiler, which infers patient-specific gene regulatory networks from a dataset of cancer gene expression profiles. NetworkProfiler is based on a statistical graphical model with varying coefficients and a kernel-based data integration method with elastic net regularization for parameter estimation. A key feature of NetworkProfiler is that the strengths of the relationships between genes are allowed to vary depending on cancer characteristics, such as cancer progression, metastasis, disease-free survival, and drug sensitivity. NetworkProfiler groups samples according to the specific cancer characteristics so that neighboring samples have common gene regulatory systems. Then, by integrating the gene expression profiles of neighboring samples with a kernel method, NetworkProfiler produces a gene regulatory network for each sample. Finally, we analyzed 2 post-analysis to discover upstream regulatory genes and downstream target genes for specific cancer characteristics. Network-

Profiler is the first algorithm for constructing patient-specific gene regulatory networks from clinical cancer gene expression data to elucidate cancer heterogeneity.

We applied NetworkProfiler to gene expression microarray data from 762 cancer cell lines to determine system changes related to the epithelial-mesenchymal transition (EMT). The epithelial-mesenchymal transition (EMT) is a process that changes proliferating cells from an aplanetic state to a motile state [5], which allows cancer cells to leave the primary tumor and metastasize. The loss of E-cadherin, a cell adhesion molecule, is a biomarker of EMT [5]. NetworkProfiler identified 25 key regulators of E-cadherin, of which half have been previously described and the other half were novel candidates. NetworkProfiler also revealed regulatory changes in *miR-141*, *ZEB1*, and E-cadherin. Specifically, our results suggested that decreased expression of *miR-141* in mesenchymal cells disrupts the negative feedback loop between *miR-141* and *ZEB1*, which would allow *ZEB1* to decrease the expression of E-cadherin during the EMT. In addition, we predicted 45 EMT-dependent putative master regulators that control sets of genes involved in cell adhesion, migration, invasion and metastasis, namely, 17 of which are downstream targets of TGFB1, a master switch of the EMT. To further validate the performance of NetworkProfiler, we experimentally evaluated *in silico* predictions obtained by NetworkProfiler. We consequently found that knockdown of KLF5, a new candidate regulator of E-cadherin, decreased E-cadherin expression and induced morphological changes characteristic of EMT. In addition, the functional involvement of miR-100 was validated in some EMT-related aspects, which was consistent with the predictions obtained by Network Profiler.

Results

Overview of NetworkProfiler

Here, we provide an overview of NetworkProfiler; please refer to the Methods section for a complete description. NetworkProfiler is a modulator-dependent graphical model because it includes a modulator (M) variable in addition to regulator (R) and target (T) variables (genes). R controls the transcription of T and M is a cofactor that modulates the interaction between R and T. In this study, we defined M as a biological or a clinical feature that is related to cancer, such as drug response, survival risk, or a molecule or pathway that is related to cancer initiation, progression, or metastasis. The relationships between R, T, and M are illustrated in Figure 1a. As shown in Figure 1b, the strength of the relationship between R and T varies depending on the value of M. Thus, M does not affect R and T directly; instead, it influences the strength of the relationship between R and T. In contrast, existing graphical models, such as Bayesian networks and mutual information networks [4], do not consider the effect of M (Figure 1c), so the strength of the relationship between R and T remains constant for all values of M (Figure 1d).

In addition, NetworkProfiler can infer the relationships between R and T, given a value of M. As a result, we could use NetworkProfiler to construct patient-specific networks with varying R-T relationships that reflect changes in the feature of interest in cancer patients. A simple example with synthetic data for R, T, and M is shown in Figure 2a. In this example, we assume that R regulates T only with a high value of M (Figure 2b). In this case, most existing methods that only consider R and T in all of the samples (Figure 2c) and ignore M would conclude that R does not regulate T. In contrast, NetworkProfiler attempts to quantify the strength of the relationship between R and T for a specific value m of M by reweighting the data according to the value of M to identify the neighborhood of samples with values of M that are close to m. Then, NetworkProfiler measures the dependency between R and T on the basis of these neighboring samples. The optimization of the size of the neighborhood is explained in the Method section.

A schematic representation of the entire analytical process of NetworkProfiler is shown in Figure 3. NetworkProfiler used 2 inputs: (1) gene expression data and (2) the modulator for each sample (Figure 3a). The gene expression data was represented as a $p \times n$ matrix, where p is the number of genes and n is the number

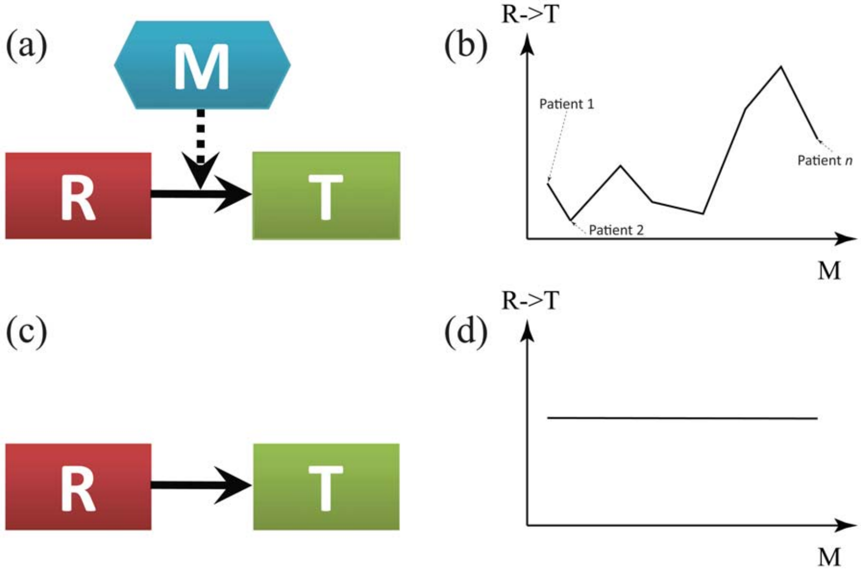

Figure 1. The relationships between a regulator (R), a target(T), and a modulator (M) in NetworkProfiler and existing graphical models. (a). The relationships between R, T and M in NetworkProfiler. The directed solid-line edge from R to T represents "R regulates the transcript of T". The directed dot-line edge from M to the edge between R and T describes "M controls the strength of the relationship between R and T". (b). The strength of the relationship between R and T in NetworkProfiler that varies depending on the value of M. (c). The relationships between R and T in existing graphical models that do not consider the effect of M. (d). The strength of the relationship between R and T in existing graphical models that remains constant for all values of M.
doi:10.1371/journal.pone.0020804.g001

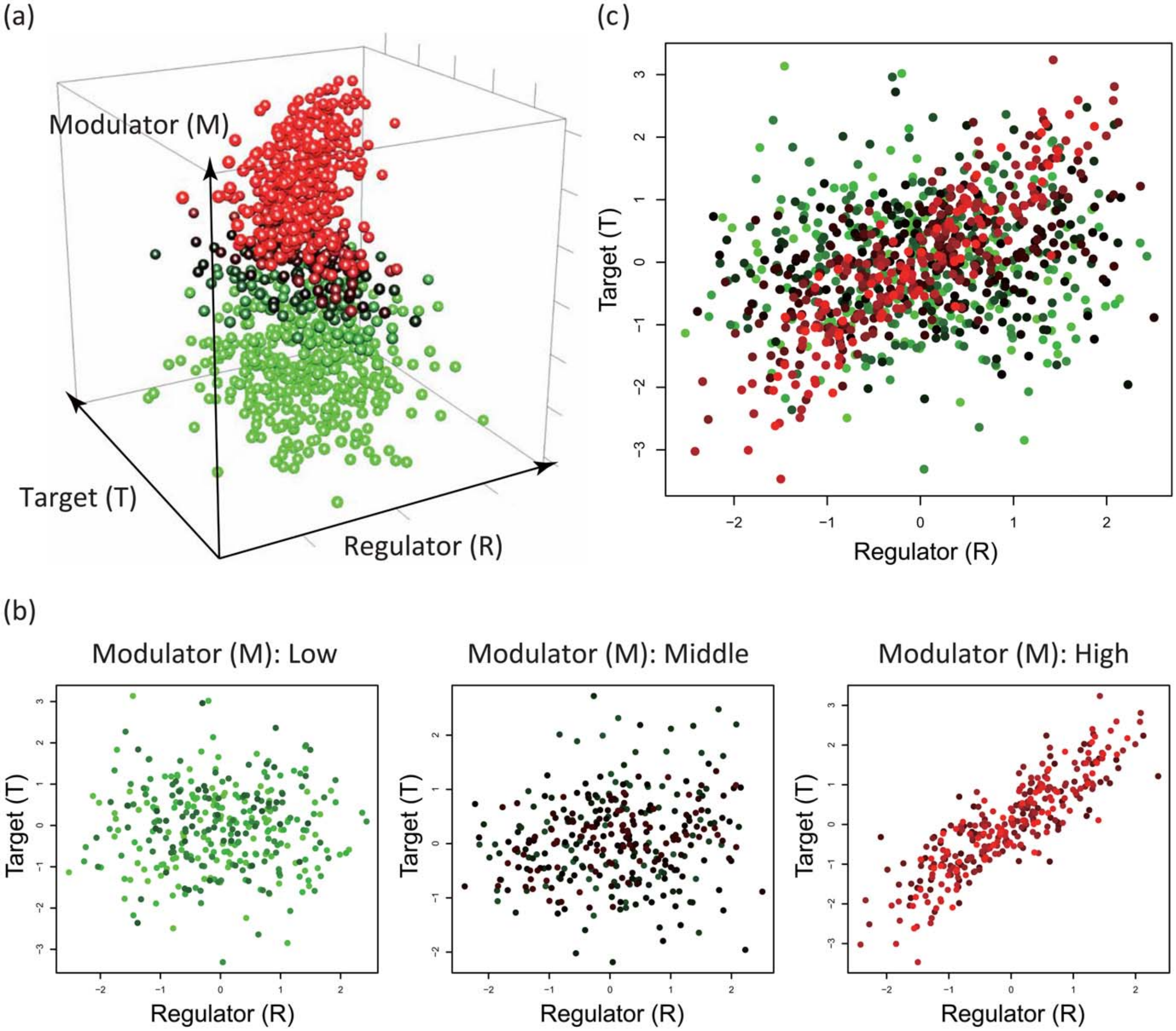

Figure 2. A regulatory change between a regulator (R) and a target (T) depending on the value of a modulator M. (a). A simple example with synthetic data from 1000 samples for R, T, and M where x-, y-, and z-axises correspond to the expressions of R and T, and the values of M, respectively. (b). The 3 scatter plots of R and T that are conditioned on the value of M. The left, middle, and right figures represent the scatter plots from 1-st sample to 333-th sample, from 334-th sample to 666-th sample, and from 667-th sample to 1000-th sample in order of ascending M, respectively. (c). The scatter plot of R and T that are not conditioned on the value of M.
doi:10.1371/journal.pone.0020804.g002

of samples (patients). If the modulator was an observable variable, then we directly applied NetworkProfiler to these inputs. However, if the modulator was a variable that is difficult to observe, then we used a signature-based hidden modulator extraction algorithm to estimate the value of the modulator. The output of NetworkProfiler is a set of gene networks for every value of M (i.e., sample-specific gene networks) shown in Figure 3b.

Afterwards, we used 2 post-analysis techniques to extract biological information from the networks. The first technique identified upstream regulators of a target gene of interest in the constructed modulator-dependent gene networks. To evaluate the modulator-dependent strength of a regulator for the target gene, we created a measure called the regulatory effect. The regulatory effect profiles of the upstream regulators for specific target genes are shown in Figure 3c. The second technique discovered putative master regulators that control downstream target gene sets with previously curated functions. To evaluate the enrichment of the target genes on a functional gene set, we created measure called the enrichment score. The resulting regulator-function matrix (Figure 3d) illustrates the candidate regulators (rows) of functions (columns) that are enhanced in the target genes.

Identification of system changes in the epithelial-mesenchymal transition

To identify system changes during the EMT, we applied NetworkProfiler to gene expression profiles of 762 cancer cell lines from the Sanger Cell Line Project (http://www.broadinstitute.org/cgi-bin/cancer/datasets.cgi). This dataset included the expression profiles of 22,777 probes, which correspond to 13,006 mRNAs in these cancer cell lines from the Affymetrix GeneChip

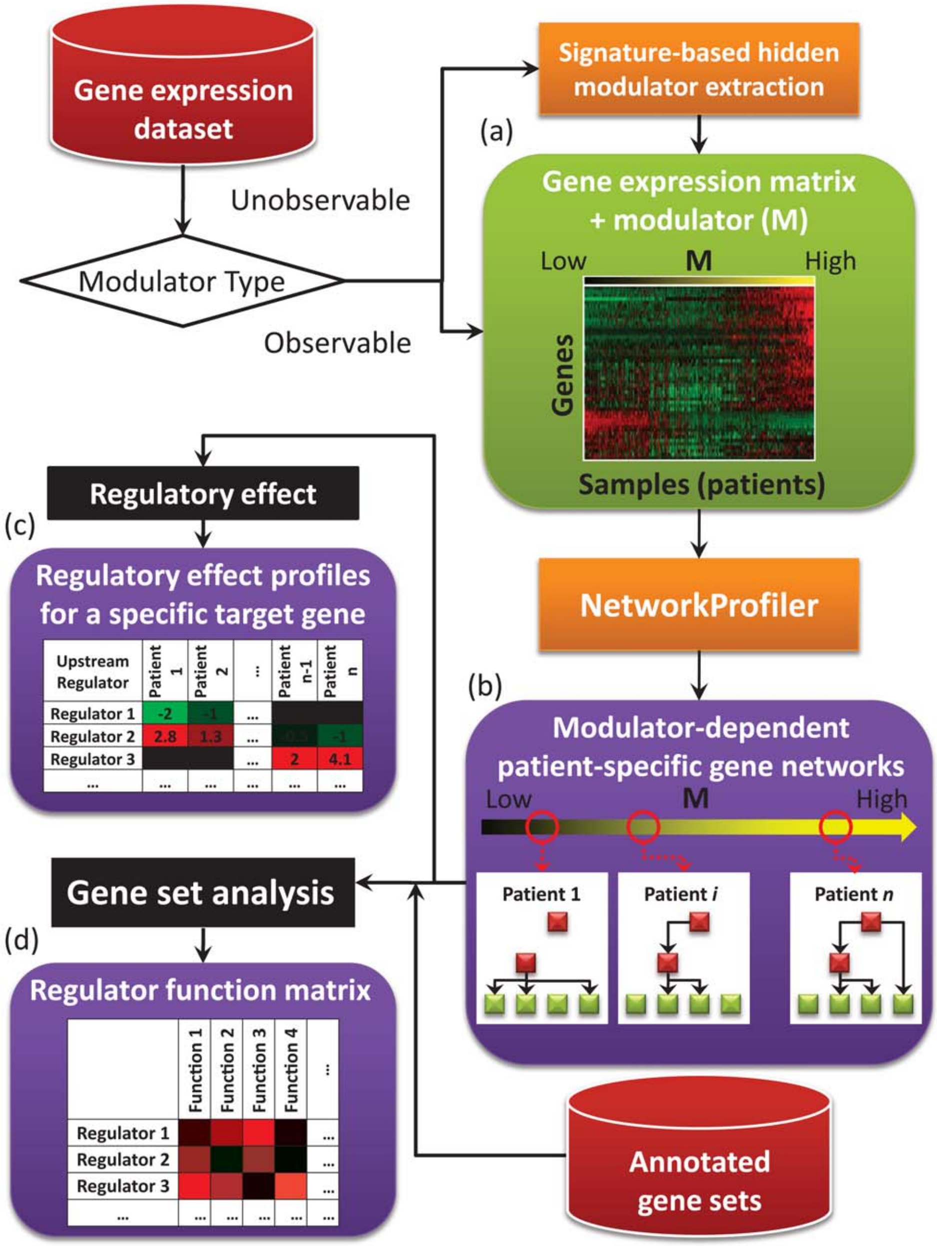
Gene expression dataset
Unobservable
Modulator Type
Observable
Signature-based hidden modulator extraction
(a)
Gene expression matrix + modulator (M)
Low
M
High
Genes
Samples (patients)
NetworkProfiler
(b)
Modulator-dependent patient-specific gene networks
Low
M
High
Patient 1
Patient *i*
Patient *n*
Regulatory effect
(c)
Regulatory effect profiles for a specific target gene
Gene set analysis
(d)
Regulator function matrix
Annotated gene sets

Upstream Regulator	Patient 1	Patient 2	...	Patient n-1	Patient n
Regulator 1	-2	-1	...		
Regulator 2	2.8	1.3	...	-0.5	-1
Regulator 3			...	2	4.1
...	...	...	...	...	...

	Function 1	Function 2	Function 3	Function 4	...
Regulator 1	⬛	🟥	🟥	⬛	...
Regulator 2	🟥	⬛	🟥	⬛	...
Regulator 3	🟥	🟥	⬛	🟥	...
...	...	...	...	...	...

Figure 3. A schematic representation of the entire analytical process of NetworkProfiler. (a). Inputs of NetworkProfiler: gene expression data matrix and the modulator for each sample. (b). Outputs of NetworkProfiler: a set of gene networks for every value of M (i.e., sample-specific gene networks). (c). The regulatory effect profiles of the upstream regulators for a specific target gene. (d). The resulting regulator function matrix whose columns are the candidate regulators and rows are functions that are enhanced in the target genes.
doi:10.1371/journal.pone.0020804.g003

Human Genome U133 Array Set (HG-U133A) and the expression profiles of 502 human microRNAs from bead-based oligonucleotide arrays. The MAS5-normalized mRNA dataset was further transformed to the log scale and quantile-normalized. During the mapping of the probes to genes, we selected 1 probe for each gene that had the largest variance, which produced a final 13,508 (genes) × 762 (cancer cell lines) gene expression matrix.

In this study, we considered transcription factors, nuclear receptors, and microRNAs to be potential regulators. To identify transcription factors and nuclear receptors, we selected human genes that were annotated as a "transcription regulator" or "ligand-dependent nuclear receptor" from the Ingenuity Knowledge Base (IKB; http://www.ingenuity.com). We also included some transcription factors that were not annotated in the IKB but were annotated in the Biobase Knowledge Library (BKL; http://biobase-international.com/). We mapped a total of 1230 genes in the HG-U133A microarray gene set to 1183 transcription factors and 47 nuclear receptors (Table S1). In addition, we included 502 human miRNA probes (Table S2).

To calculate the modulator values for the EMT in the 762 cancer cell lines, we applied a signature-based hidden modulator extraction algorithm (see Methods for details) to the expression data. First, we selected 122 genes labeled "EMT_UP", "EMT_DN", "JECHLINGER_EMT_UP", and "JECHLINGER_EMT_DN" from Molecular Signatures Database v2.5 ([6]; http://www.broadinstitute.org/gsea/msigdb/index.jsp). Then, this algorithm narrowed the set to

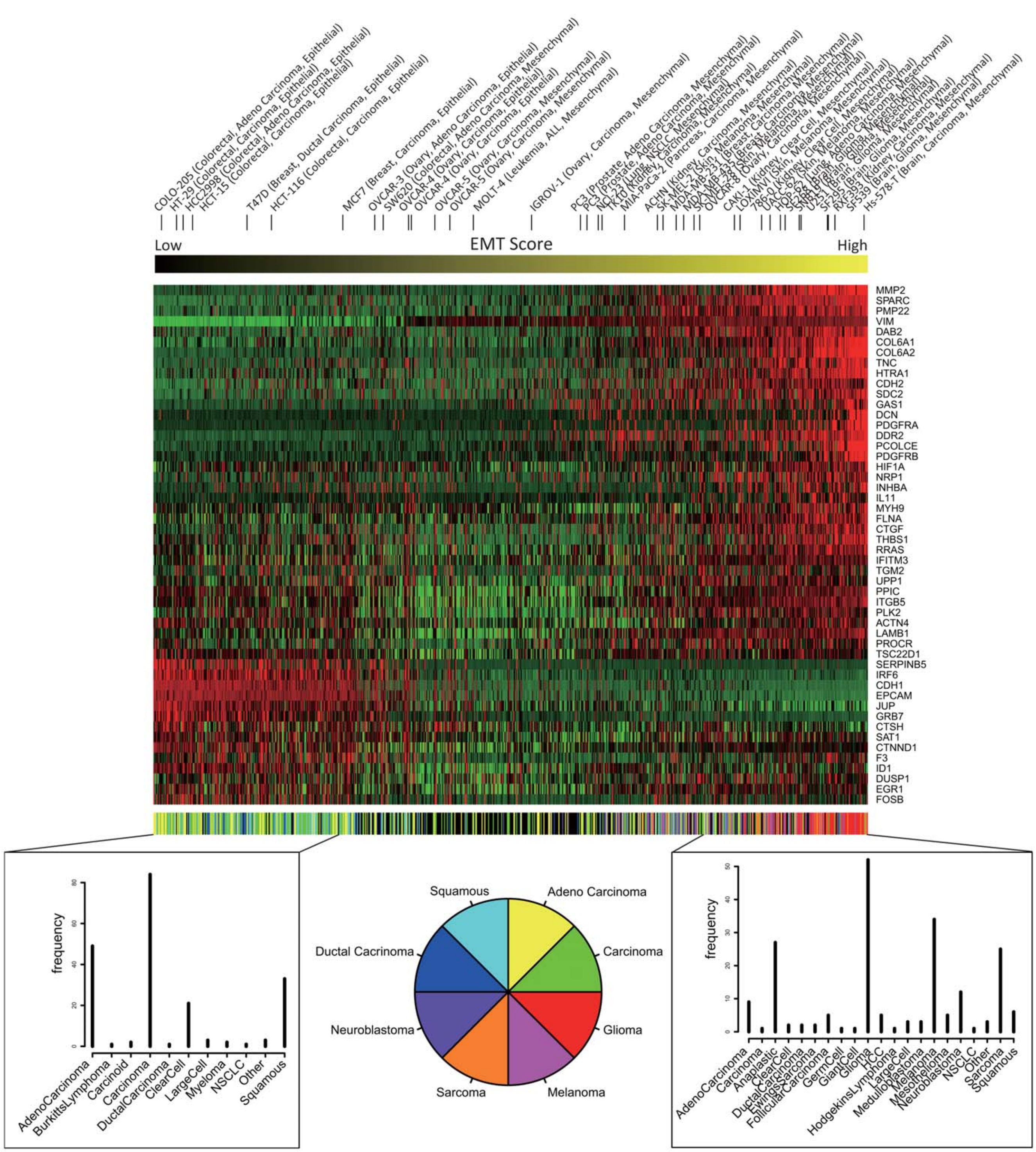

Figure 4. Expression profiles of the 50 functionally coherent genes in ascending order of the EMT-related modulator values. The heatmap represents normalized expression profiles so that the mean and variance for each gene are 0 and 1, respectively. The red color represents positive expressions and the green color represents negative expressions. The upper strings indicate cell line names which are known to be epithelial or mesenchymal. The upper horizontal color bar represents the values of the EMT-related modulator with the signature-based hidden modulator extraction algorithm. The bottom horizontal color bar shows primary histories of 762 cancer cell lines whose color corresponds to one of the eight primary histories or the other histories (black). The bottom histograms represent frequencies of the primary histories between samples with the 200 lowest and 200 highest values of the EMT-related modulator, respectively.

doi:10.1371/journal.pone.0020804.g004

50 functionally coherent genes with $p < 10^{-5}$ by using the extraction of expression module (EEM) [7] (Table S3) and computed the first principal component of these 50 genes as hidden values of the EMT-related modulator (Table S4). Since the direction of the first principal component did not always correspond to that of the EMT, we changed the sign of the modulator values by

multiplying either plus or minus one so that epithelial-like cells have lower modulator values than mesenchymal-like cells.

Figure 4 shows the expression profiles of the 50 functionally coherent genes in ascending order of the EMT-related modulator values. These modulator values clearly discriminated cell lines that were epithelial-like or mesenchymal-like. Specifically, cells with smaller or larger modulator values had more epithelial or mesenchymal phenotypes, respectively. Furthermore, many carcinomas and squamous tumors had low modulator values, while many gliomas and melanomas had high values. By using these EMT-related modulator values, NetworkProfiler constructed 762 regulatory gene networks that are related to the EMT. The list of the estimated edges in each of these networks can be downloaded from the supporting web site (Files S1, S2, and S3; http://bonsai.hgc.jp/~shima/NetworkProfiler).

Identification of regulators of E-cadherin that induce the epithelial-mesenchymal transition

To identify possible regulators that might control the expression of E-cadherin during the EMT, we calculated the regulatory effects of the upstream regulators of E-cadherin. Out of 1732 potential regulators, NetworkProfiler inferred that 370 of them may control the expression of E-cadherin in any of the 762 cancer cell lines (Table S5). These putative regulators were ranked according to the change in their regulatory effect during the EMT. Although we did not include any information on known E-cadherin regulators, about half of the 25 highest ranked regulators were previously reported in the literature (Table 1). For example, 2 zinc finger transcription factors, ZEB1 and ZEB2, are direct repressors of E-cadherin and are involved in the EMT [9,15]. In addition, the miR-200 family indirectly suppresses the EMT by inhibiting the translation of ZEB1 and ZEB2 mRNAs [8]. Similarly, miR-192 inhibits the translation of ZEB2 [13,14]. In addition, SNAI2, a member of the Snail superfamily of zinc finger transcription factors, also is involved in the EMT [16]. Likewise, TCF4 (also known as E2-2), a class I bHLH transcription factor, is an EMT regulator; its isoforms induce the EMT in MDCK kidney epithelial cells [12]. In contrast, FOXA1 and FOXA2 are positive regulators of E-cadherin, which suppress the EMT in pancreatic ductal adenocarcinoma [11]. KLF4 also inhibits the EMT by regulating E-cadherin expression [10]. NetworkProfiler also identified several other known direct repressors of E-cadherin, such as TWIST1 [17] and TCF3 (also known as E47) [18]; however, these regulators were ranked 38th and 84th, respectively.

The other half of the 25 highest ranked regulators has not yet been reported and may be novel EMT-dependent regulators of E-cadherin. For example, although the relationship between GRHL2 and EMT is not known, GRHL2 is required for morphogenesis of epidermal and tracheal cells and plays an important role in regulating the expression levels of E-cadherin in *Drosophila* post-embryonic neuroblasts [19]. ZNF217 binds the E-cadherin promoter [20], which suggests that ZNF217 might be a transcription factor for E-cadherin.

Next, we compared the performance of NetworkProfiler with that of a structural equation model (SEM) of E-cadherin that was inferred by the elastic net [22]. This model was equivalent to a regression model where the response variable is the expression of E-cadherin and the explanatory variables are the 1732 regulator expressions. The significance of each regulator was evaluated based on the number of non-zero regression coefficients in 1000 bootstrapped datasets. The SEM inferred 627 putative regulators (Table S6). Among these putative regulators, there were only 6 regulators, namely, *ZEB1*, *miR-141*, *ZEB2*, *TCF3*, *miR-200b*, and *miR-200c*, in the 25 highest ranked regulators that were previously reported in the literature. This result suggested that NetworkProfiler was superior to the traditional gene network estimation methods to identify regulators of E-cadherin that are involved in the EMT. Moreover, NetworkProfiler can reveal regulatory changes among genes during the EMT. Figures 5a and 5b show the regulatory profiles of putative regulators of E-cadherin when the lengths of the paths from the regulators to E-cadherin is 1 and 2, respectively.

NetworkProfiler can also predict mechanistic interpretations of published experiments. For example, it is known that ZEB1 and ZEB2 induce EMT by repressing E-cadherin transcription and that ectopic expression of the miR-200 family (miR-200a, miR-200b, miR-200c, and miR-141) or miR-205 leads to downregulation of ZEB1 and ZEB2, upregulation of E-cadherin, and mesenchymal-epithelial transition (MET) in cells [8]. As the relationships between these genes, the prediction of NetworkProfiler provides the following results. As shown in Figures 6c and 6d, although the expression of miR-141 had a strong positive effect on that of E-cadherin in epithelial-like cells, this effect decreases during the EMT. In contrast, although the expression of ZEB1 had a weak negative effect on that of E-cadherin in epithelial-like cells, this effect increased during the EMT. Interestingly, miR-141 and ZEB1 had a strong, direct

Table 1. 25 top-ranked regulators of E-cadherin for the change in the regulatory effect change among the EMT with published evidence.

regulator	type	regulatory effect change	Evidence
IRF6	A	101.04	
miR-141	A	87.58	[8]
GRHL2	A	64.13	
ZEB1 (SIP1)	I	50.72	[9]
LSR	I	46.89	
miR-200b	A	31.55	[8]
KLF4	A	26.28	[10]
OVOL2	A	22.08	
miR-200a	A	17.70	[8]
FOXA2	A	17.26	[11]
TCF4 (E2.2)	I	14.15	[12]
ELF3	A	13.58	
ZNF217	A	13.53	
MYB	A	12.50	
KLF5	A	12.42	
miR-192	A	12.30	[13, 14]
FOXA1	A	11.69	[11]
ZNF165	A	11.39	
NKX2-1	A	11.21	
HNF1B	A	11.08	
TFE3	A	11.01	
ZEB2 (δEF)	I	10.66	[15]
TRIM29	I	9.87	
SNAI2	I	9.74	[16]

The labels "A" and "I" indicate 2 types of the regulator: activator (A) and inhibitor (I). See Table S5 for the complete table of the 370 putative regulators for E-cadherin.

doi:10.1371/journal.pone.0020804.t001

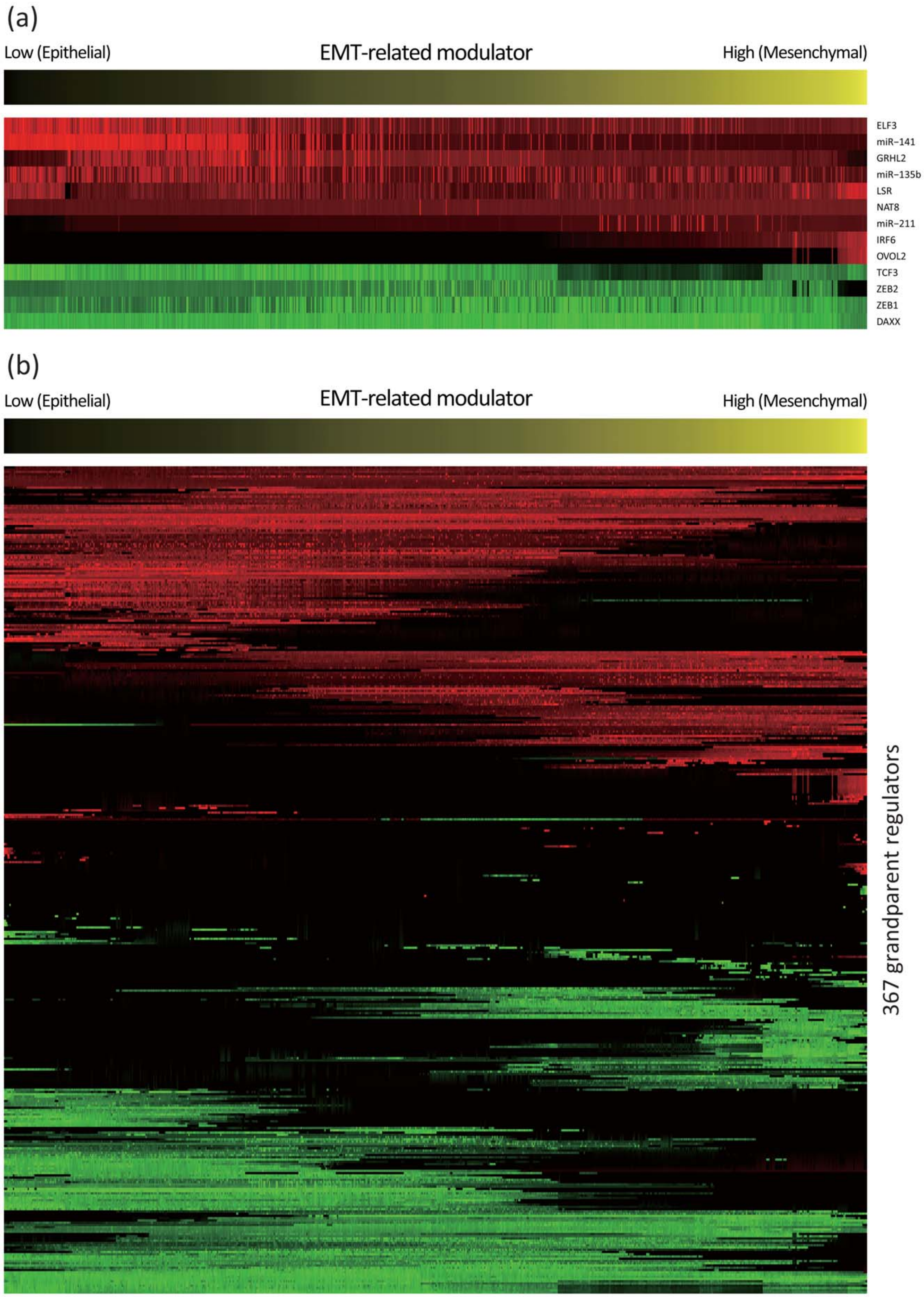
(a)
Low (Epithelial)
EMT-related modulator
High (Mesenchymal)
ELF3
miR−141
GRHL2
miR−135b
LSR
NAT8
miR−211
IRF6
OVOL2
TCF3
ZEB2
ZEB1
DAXX
(b)
Low (Epithelial)
EMT-related modulator
High (Mesenchymal)
367 grandparent regulators

Figure 5. Regulatory effect profiles of the putative regulators of E-cadherin among the EMT. (a). The regulatory effect profiles of the 13 putative regulators among the EMT when the length of the paths from the regulators to E-cadherin is 1 where rows indicate the putative regulators of E-cadherin and columns indicate samples (cancer cell lines). The positive (red) and negative (green) regulatory effect indicate that the parent regulator controls the transcript of E-cadherin positively and negatively, respectively. (b). The regulatory effect profiles of the 13 putative regulators among the EMT when the length of the paths from the regulators to E-cadherin is 2.
doi:10.1371/journal.pone.0020804.g005

negative effect on each other only when the EMT-related modulator values were low. This implied that there is a negative feedback loop between miR-141 and ZEB1 in epithelial-like cells, which is consistent with a previous study [23]. Furthermore, during the EMT, the expression levels of miR-141 and E-cadherin decreased, while the expression level of ZEB1

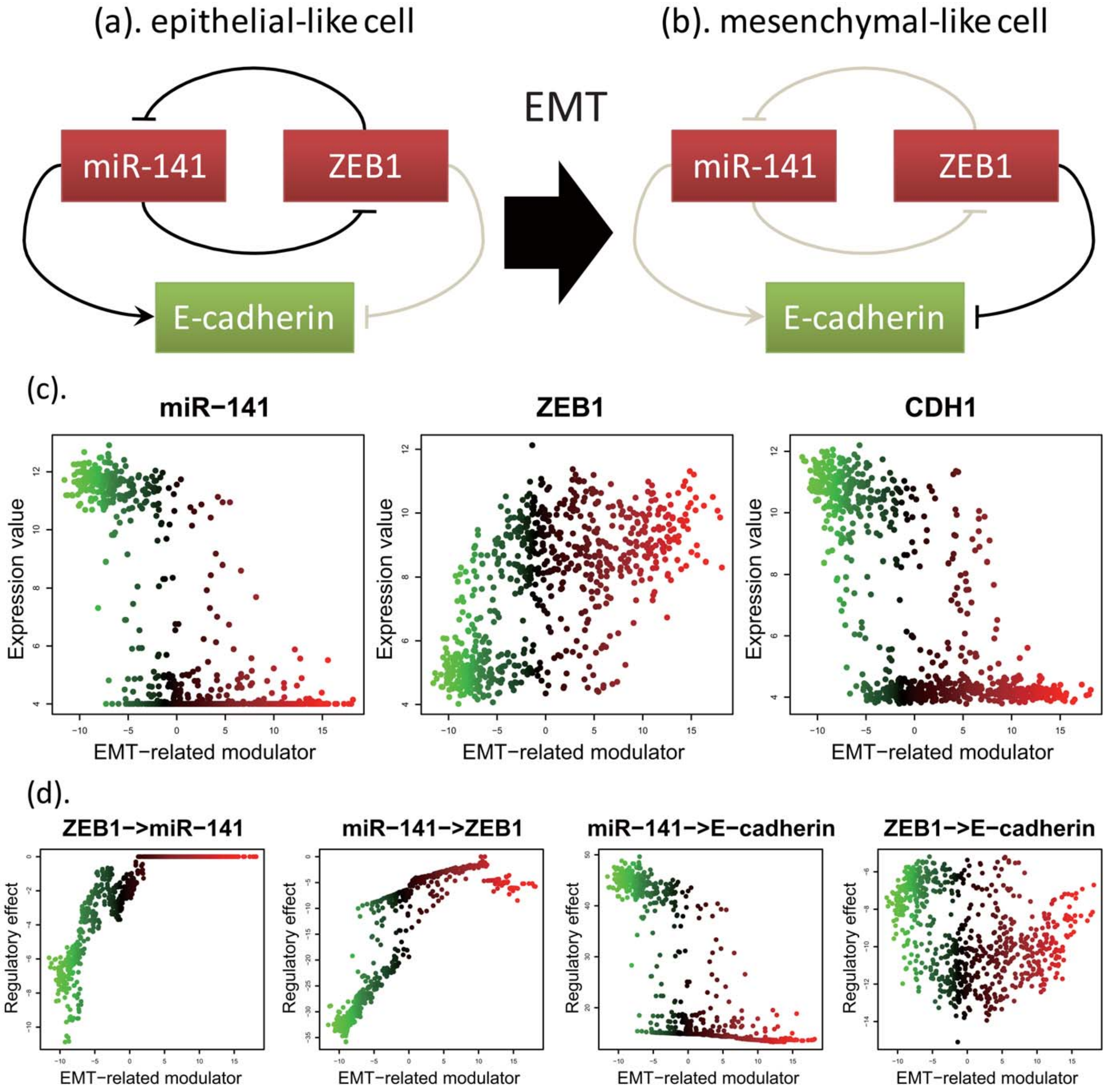

Figure 6. Regulatory changes among miR-141, ZEB1, and E-cadherin among the EMT. (a). The relationship among miR-141, ZEB1, and E-cadherin in epithelial-like cells. (b). The relationship among miR-141, ZEB1, and E-cadherin in mesenchymal-like cells. (c). The expression profiles of miR-141 (left), ZEB1 (middle), and E-cadherin (right) in order of ascending the EMT-related modulator values. The green and red colors indicate epithelial- and mesenchymal-like cells, respectively. (d). The regulatory effects from ZEB1 to miR-141, from miR-141 to ZEB1, from miR-141 to E-cadherin, and from ZEB1 to E-cadherin when the length of the paths is 1.
doi:10.1371/journal.pone.0020804.g006

Table 2. Selected relationships between the 47 putative master regulators and the 5 functional categories with published evidence.

regulator	function	$-\log_{10}(q\text{-value})$	mode of action (E⇒M)					evidence
			A⇑	A⇓	I⇑	I⇓	–	
FOSL1	migration	9.82	29	2	42	3	41	[25]
	invasion	8.42	14	2	24	3	22	[26]
EPAS1	adhesion	5.90	26	1	10	0	16	[27]
	migration	7.66	32	1	14	0	24	[28]
KLF5	migration	5.93	28	2	27	5	25	[29]
AHR	metastasis	3.67	12	0	11	0	9	[30]
FOXF1	metastasis	6.10	24	0	9	0	8	[31]
	migration	6.09	29	0	17	0	14	[32]
ELK3	migration	6.23	41	8	17	7	19	[33]
SMAD3	adhesion	4.57	9	3	23	0	10	[34]
	metastasis	3.12	5	1	12	1	9	[35]
	migration	5.24	14	5	26	1	21	[36]
	EMT	2.47	1	1	2	0	0	[37]
WWTR1	migration	5.08	32	0	17	3	16	[38]
	invasion	3.48	17	0	8	2	5	[38]
hsa-miR-145	invasion	2.52	13	0	8	3	17	[39]
CEBPD	metastasis	4.88	17	2	10	0	9	[31]
TGFB1I1	adhesion	5.12	25	2	23	5	11	[40]
HIF1A	adhesion	3.84	10	0	25	3	10	[27]
	metastasis	4.45	14	1	14	0	8	[41]
	migration	5.00	18	3	25	4	21	[42]
	invasion	3.65	12	0	9	3	10	[43]
SNAI2	migration	3.45	36	2	25	14	25	[25]
ELF3	adhesion	7.87	24	4	24	11	14	[44]
	invasion	4.45	9	3	18	6	21	[44]
SOX9	adhesion	6.80	18	2	19	0	26	[45]
	migration	5.46	28	2	15	1	23	[46]
GLI3	migration	4.53	24	7	24	7	26	[47]
TCF7L2	migration	4.52	19	10	18	1	27	[48]
NFKBIA	adhesion	2.73	12	2	14	3	12	[49]
	metastasis	2.39	5	0	5	3	9	[50]
	migration	3.98	18	2	18	7	23	[51]
	invasion	2.69	9	2	5	2	12	[50]
VAV1	adhesion	5.51	3	5	15	3	14	[52]
	migration	5.10	7	10	16	5	16	[53]
JUN	adhesion	3.03	15	4	6	5	6	[54]
	migration	3.31	19	2	7	7	14	[25]
	invasion	2.07	8	2	7	2	5	[55]
ETV1	invasion	2.50	13	1	13	5	7	[56]
PDLIM1	adhesion	4.27	16	6	17	6	29	[57]
MAFB	metastasis	4.41	9	0	3	8	6	[31]
GATA6	metastasis	3.25	11	3	4	1	4	[31]
RUNX1	adhesion	6.27	15	5	16	12	14	[58]
	migration	2.46	23	7	20	7	20	[59]
YAP1	migration	3.30	7	2	20	0	9	[60]

The labels "A⇑", "A⇓", "I⇑", and "I⇓", and "–" indicate the number of the five modulator modes of action for the relationship between a regulator and its target included in the functional gene set: "the activation of a regulator on the expressions of its target genes with the functional category was increased by the modulator", "inhibition increased", "activation decreased", "inhibition decreased", and "the modulator mode of action is not determined", respectively.

doi:10.1371/journal.pone.0020804.t002

increased. These results suggested that reduced expression of miR-141 disrupts the negative feedback loop between miR-141 and ZEB1 (Figures 6a and 6b), which would allow ZEB1 to decrease the expression of E-cadherin, as illustrated in Figure 6c. It should be noted that these results cannot be predicted by traditional graphical models which infer a static gene network structure.

Identification of relationships between regulators and epithelial-mesenchymal transition-related functional gene sets

The EMT-dependent relationships between downstream target genes for each regulator and previously curated functional gene sets in each sample were analyzed by applying gene set analysis (see Methods for details) to the constructed gene networks for 762 cancer cell lines. We tested five curated gene sets included in Ingenuity Knowledge Base (IKB; http://www.ingenuity.com). These gene sets were related with *adhesion*, *migration*, *invasion*, and *metastasis* which were hallmarks of EMT [5], and EMT itself. By using gene set analysis, the statistical significances (q-values) for the enrichments of downstream genes for the 1732 regulators on the five functional gene sets were calculated in each of the 762 cell lines. These results can be downloaded from the supporting web site (File S4; http://bonsai.hgc.jp/~shima/NetworkProfiler).

To search for regulators that strongly affected the five EMT-related functional gene sets, the change in the enrichment score during the EMT and their integral q-value were calculated. The result was summarized by a regulator function matrix (Table S7). We focused on 45 regulators with the integral q-values less than 10^{-10} as putative master regulators that strongly enhanced the

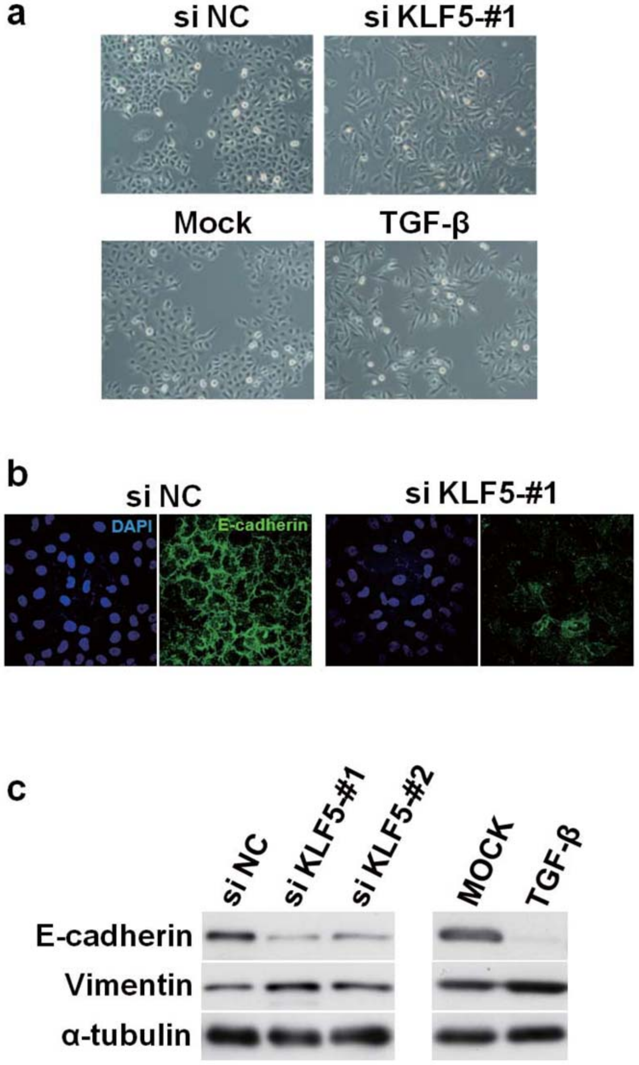

Figure 7. Induction of EMT by KLF5 knockdown in A549 NSCLC cell line. (a) Phase contrast images of A549 cells 72 hours after siRNA transfection, showing a fibroblast-like morphology in siKLF5 treated cells. TGF-β treatment serves as a positive control for EMT induction in A549 cells. (b) Representative immunofluorescence staining images, showing reduced E-cadherin expression in siKLF5-treated A549 cells. (c) Western blot analysis of E-cadherin and vimentin, showing EMT-related changes in their expression in A549 cells treated with two differenct siRNAs.
doi:10.1371/journal.pone.0020804.g007

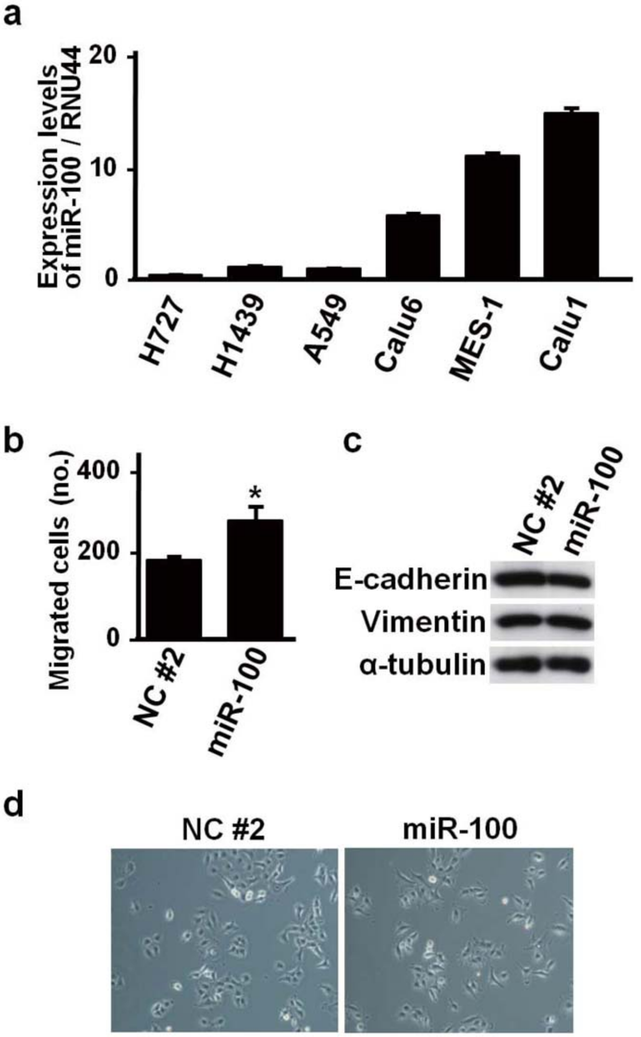

Figure 8. miR-100-induced changes in biologic characteristics in A549 NSCLC cell line. (a) Quantitative real-time RT-PCR analysis of miR-100 in six NSCLC cell lines, showing low miR-100 expression in A549, NCI-H727 and NCI-H1437. (b) Motility assay showing increased migration in miR-100-transfected A549 cells. Error bars indicate SE in three independent experiments (*, $p < 0.05$). NC#2, negative control. (c) Western blot analysis of E-cadherin, vimentin and α-tubulin, showing lack of noticeable changes in miR-100-transfected A549 cells (d) Representative phase contrast microscopic images showing negligible changes in miR-100-trasfected A549 cells.
doi:10.1371/journal.pone.0020804.g008

functional gene sets related with the EMT. Interestingly, among the 45 regulators, 17 regulators were downstream targets of transforming growth factor β-1 (TGFB1), a master switch of EMT [24], with published evidence (Table S8). This result suggests that these regulators have crucial roles in TGFB1-induced EMT.

As a control, we tested how well the NetworkProfiler analysis identified known relationships between regulators and functional gene sets in the Ingenuity Knowledge Base. The known functional relationships of the 45 putative master regulators are shown in Table 2. For example, FOSL1 increases the migration of MDA-MB-436 cells [25] and the invasion of A549 cells [26]. SMAD3 increases the adhesion [34], the metastasis [35], and the migration [36] of cells, respectively. Similarly, HIF1A increases the adhesion of undifferentiated trophoblast stem cells [27], the metastasis of LM2 cells [41], the migration of HUVEC cells [42], and the invasion of Achn cells [43], respectively.

Although some of the 47 putative master regulators have not been reported to enhance the EMT-related functions in IKB, some predictions were supported by other resent works which were not included in IKB. For example, the prediction of NetworkProfiler suggested that PTRF regulates gene sets related with migration (q-value $= 2.45 \times 10^{-8}$) and with metastasis (q-value $= 2.03 \times 10^{-6}$) during the EMT. Consistent with the *in silico* result, PTRF expression inhibits migration and correlates with metastasis in PC3 prostate cancer cells [61]. Similarly, NetworkProfiler predicted that miR-146 contributes to migration (q-value $= 3.27 \times 10^{-9}$) and invasion (q-value $= 1.01 \times 10^{-4}$) during the EMT. This *in silico* result is comparable with the *in vitro* result that miR-146 inhibits invasion and migration, and acts as a metastasis suppressor [62]. In addition, some predictions between miRNAs and functions seem reasonable based on the known functions of the miRNA host genes. For example, the prediction of NetworkProfiler provided the hypothesis that miR-143 and miR-145 promotes metastasis (q-value $= 7.17 \times 10^{-4}$ and 3.15×10^{-5}) and migration (q-value $= 1.37 \times 10^{-6}$ and 6.10×10^{-8}), respectively. miR-143 and miR-145 cooperatively target a network of transcription factors, such as KLF4, to control smooth muscle phenotype switching [63]. Since KLF4 increases the migration of cells [29] and induces EMT [10], these miRNAs might be related with EMT-related functions or control EMT by targeting KLF4. Again, it should be noted that these relationships between regulators and functions cannot be predicted from one gene network constructed by traditional graphical models, and only the results of multiple network comparison between epithelial-like and mesenchymal-like cells based on NetworkProfiler enables us to support the recent biological knowledge and new hypotheses about unknown relationships.

Comparison between *in silico* predictions and *in vitro* results

To validate the performance of NetworkProfiler, *in silico* predictions obtained by NetworkProfiler were evaluated experimentally. We first conducted *in vitro* experiments of a new candidate regulator of E-cadherin listed in Table 1, KLF5, to investigate whether KLF5 affects E-cadherin expression and induces morphologic changes characteristic of EMT using A549 lung adenocarcinoma cell line, which is well known to exhibit EMT in response to TGF-β [64]. KLF5 knockdown markedly altered a cobblestone epithelial morphology of A549 cells and induced a more fibroblast-like morphology with reduced cell-cell contact, which was similar to that seen in TGF-β-treated A549 cells (Figure 7a and Figure S1). Immunofluorescence analysis showed significant reduction of E-cadherin expression in A549 cells knocked down for KLF5 (Figure 7b), which was also confirmed by western blot analysis (Figure 7c). Conversely, vimentin expression was shown to be modestly increased by siKLF5 treatment (Figure 7c). Consistent with the *in vitro* results, the prediction of NetworkProfiler suggested that KLF5 affects E-cadherin expression as well as Vimentin expression during the EMT, since the changes in the regulatory effects from KLF5 to E-cadherin and Vimentin were much larger compared with the other regulators (12.42 and 16.57, respectively) which was ranked 15-th and 10-th among the 1732 regulators (Table S9). The result of gene set analysis (Table S7) also suggested that KLF5 affects EMT (q-value $= 1.60 \times 10^{-24}$). Thus, we consequently found that *in silico* predictions obtained by NetworkProfiler was confirmed with the results of *in vitro* experiments; KLF5, a newly identified candidate regulator of EMT, was shown to affect expressions of E-cadherin and Vimentin as well as morphologic characteristics related to EMT as a repressor of EMT.

We also conducted *in vitro* experiments to validate functional involvement of a novel candidate EMT-related microRNA, miR-100 whose expression was increased in 762 cancer cell lines during the EMT (Figure S2). miR-100 was found to be expressed at a low level in A549, NCI-H727 and NCI-H1439 NSCLC cell lines, which had low EMT-related modulator values among the 762 cell lines panel (Figure 8a). miR-100 was transiently introduced into A549 cells, resulting in a significant increase of cell migration activity (Figure 8b). However, overexpression of miR-100 did not affect expressions of an epithelial marker, E-cadherin, and a mesenchymal marker, vimentin (Figure 8c), and also did not influence cell morphology (Figure 8d). However, overexpression of miR-100 significantly increased cell migration without noticeably affecting morphology in NCI-H727 and NCI-H1437 cells (Figure S3). Consistent with the *in vitro* results, the prediction of NetworkProfiler suggested that miR-100 enhances migration (q-value $= 1.42 \times 10^{4}$) but does not affect EMT itself (q-value $= 0.24$) from gene set analysis (Table S7). It also suggested that miR-100 does not affect the expressions of E-cadherin and Vimentin during the EMT, since E-cadherin and Vimentin were not target genes of miR-100 in all the 762 cell line-specific gene networks related with the EMT(Files S1, S2, and S3) and the changes in the regulatory effects from miR-100 to E-cadherin and Vimentin were much smaller compared with the other regulators (0 and 1.72, respectively), which were ranked 371-th and 151-th among the 1732 regulators (Table S9). Thus, we conclude that several hypotheses of miR-100 functions provided by NetworkProfiler are consistent with the results of *in vitro* experiments; NetworkProfiler has the potential to uncover novel biological mechanisms.

Discussion

We developed a novel algorithm called NetworkProfiler to infer patient-specific, modulator-dependent gene regulatory networks from gene expression data. Unlike traditional methods that infer a static network for a specific state of a cell or an averaged network for many patients, NetworkProfiler can be used to construct patient-specific gene networks for specific diseases, such as cancer. Subsequently, information about the regulatory effects of individual genes and functional gene sets can be extracted from these networks. In order to show the performance of NetworkProfiler, we applied NetworkProfiler to microarray gene expression data from 762 cancer cell lines to identify the system changes that were related to the EMT. As a result, we identified 25 EMT-dependent regulators of E-cadherin. Although some of these regulators have been reported in the literature, others may be novel master regulators of E-cadherin that induce the EMT. Moreover, in comparison to the traditional SEM approach, the performance of NetworkProfiler was superior for identifying regulators of E-cadherin during the EMT. We also showed that NetworkProfiler can reveal regulatory changes of E-cadherin during the EMT. In particular, our results suggested that decreased expression of miR-141 disrupts the negative feedback loop between miR-141 and ZEB1, which would allow ZEB1 to decrease the expression of E-cadherin.

Furthermore, we also identified putative relationships between regulators and EMT-dependent functional gene sets, some of which had published evidence. Based on the significance of the enrichment of downstream target genes for the regulator on the 5 functional gene sets, we identified 45 putative master regulators for the EMT. We found that 17 regulators were downstream targets of TGFB1 that is a master switch of the EMT. We then showed that NetworkProfiler can not only predict the relationships between these regulators and functions that were supported by many published evidence, but also produce new hypotheses that some of them might enhance EMT-related functions or induce EMT.

Finally, it is of note that we were able to validate the *in silico* predictions obtained by NetworkProfiler in our *in vitro* experiments. KLF5, a newly identified candidate regulator of EMT, was experimentally shown to affect E-cadherin expression as well as morphologic characteristics related to EMT, validating the NetworkProfiler-based prediction that KLF5 is a negative regulator of EMT. We also conducted *in vitro* experiments of another regulator, miR-100, for which NetworkProfiler predicted its association with some EMT-associated functions. As a result, we found that the predicted miR-100 functions conformed to the results of *in vitro* experiments. Thus, we conclude that the effectiveness of the proposed method was validated not only from published literature but also from new *in vitro* validation experiments.

We anticipate several possible applications and extensions of NetworkProfiler. In this study, we only focused on the system changes that are associated with the EMT. NetworkProfiler also could be used to infer system changes and reconstruct modulator-dependent gene networks for other well-defined modulators, such as drug sensitivity and prognosis risk. Currently, a significant limitation of NetworkProfiler is that the modulator must be one-dimensional. However, cancer development is a multivariate process. It may be possible to use multivariate kernel functions in NetworkProfiler to overcome this limitation.

During the past decade, cancer therapy has become increasingly personalized [2,3]. Unlike the traditional "one-size-fits-all" approach to cancer therapy, patient-specific cancer therapy reduces the side effects of chemotherapy and predicts the odds of cancer recurrence more accurately by tailoring cancer treatment to specific genetic defects in the tumors of individual patients. However, this goal is not an easy task since cancer is an extremely complex and heterogeneous disease. We believe that NetworkProfiler will help elucidate the systems biology of cancer and facilitate personalized chemotherapy.

Materials and Methods

Cell lines and reagents

Human non-small cell lung cancer (NSCLC) cell lines, A549, NCI-H1437 and NCI-H727, were purchased from American Tissue Culture Collection, while other NSCLC cell lines, Calu1, Calu6 and SK-MES1, were generously provided by Dr. L. J. Old (Memorial Sloan-Kettering Cancer Center). Cells were maintained in RPMI 1640 supplemented with 10% fetal bovine serum. The anti-E-cadherin antibody was purchased from BD Transduction Laboratories, anti-vimentin from Santa Cruz Biotechnology, anti-α-tublin from Sigma Aldrich, and anti-mouse IgG from Cell Signaling Technology. The Alexa-conjugated anti-mouse IgG was purchased from Molecular Probes. siRNAs against KLF5 (siKLF5 #1 and #2) and a negative control (siNC) were purchased from Sigma Genosys. Pre-miR has-miR-100 and negative control #2 were purchased from Ambion. Human TGF-β was purchased from R&D Systems, Inc.

Immunostaining, western blot analysis and in vitro motility assay

2×10^4 cells in 6-well plates were transiently transfected with either 20 nM siRNA or 10 nM Pre-miR molecules using Lipofectamine RNAiMAX (Invitrogen), as previously described [65]. Immunofluorescence staining was carried out after fixation with 3.7% formaldehyde and postfixing with 0.1% Triton X-100 each for 10 min at RT. Photographs were taken 72 hr after transfection. Cells were harvested 48 hr after transfection for western blot analysis. In vitro motility assay based on Transwell-chamber culture systems was performed, as previously described [66].

Quantitative real-time reverse transcription (RT)-PCR analysis

Quantitative real-time RT-PCR analysis of KLF5 was performed using Power SYBR Green (Applied Biosystems) and the following PCR primers:

5′-CCCTTGCACATACACAATGC-3′ and 5′-GGATGGAGGTGGGGTTAAAT-3′. Quantitative real-time RT-PCR analysis of miR-100 and RNU44 was performed using TaqMan probes and 7500 Fast Real-Time PCR system (Applied Biosystems), essentially as previously described [67].

NetworkProfiler

NetworkProfiler employed a varying-coefficient structural equation model (SEM) to represent the modulator-dependent conditional independence between gene transcripts. Let there be q possible regulators, $R_1,\ldots,R_q$, that may control the transcription of the k-th target gene T_k when the modulator $M=m$. Then the varying-coefficient structural equation model for T_k is

$$T_k=\sum_{j=0}^{q}\beta_{jk}(m)\cdot R_j+\varepsilon_k,$$

where $\beta_{jk}(m)$ is the coefficient function that represents the effect of R_j on T_k, $R_0=1$, and ε_k is a noise term. If $T_k=R_l$, then the term $\beta_{lk}(m)\cdot R_l$ can be omitted from the model, i.e., $\beta_{lk}(m)=0$ for all m. By estimating the parameters $\beta_{jk}(m)$, we obtain the transcriptional regulatory gene network at $M=m$.

We used a kernel-based method to estimate these parameters. Let there be n sets of gene expression profiles. Then, the SEM for the α-th sample can be rewritten as

$$t_{\alpha k}=\sum_{j=0}^{q}\beta_{jk\alpha}\cdot r_{\alpha j}+\varepsilon_{\alpha k},\alpha=1,\ldots,n,$$

where $t_{\alpha k}$, $r_{\alpha j}$, and m_α are the values of the k-th target gene, the j-th regulator, and the modulator for the α-th sample, respectively; $r_{0k}=1$, and $\beta_{jk\alpha}=\beta_{jk}(m_\alpha)$. For n samples, we obtain n modulator-dependent gene regulatory networks, i.e., the regulatory effects of R_j $(j=1,\ldots,q)$ on T_k $(k=1,\ldots,p)$ are determined by $\hat{\beta}_{111},\ldots,\hat{\beta}_{qpn}$, where $\hat{\beta}_{jk\alpha}$ is the estimate of $\beta_{jk\alpha}$.

We assumed that the values of the coefficients are almost constant for the neighborhood samples of the α-th sample with respect to the modulator m, that is, $\beta_{jki}\approx c$ for the i-th sample that satisfies $|m_i - m_\alpha| < \delta$ for some constant c and small δ. Then, we estimated the parameters $\beta_{jk\alpha}$ for fixed α by minimizing a regularized kernel-based weighted residual sum of squares

$$L_k(\beta_{1k\alpha},\ldots,\beta_{qk\alpha}|h_k) = \frac{1}{2}\sum_{i=1}^{n}\{t_{ik} - \sum_{j=1}^{q}\beta_{jk\alpha}\cdot r_{ij}\}^2 K(m_i - m_\alpha|h_k)$$

$$+\lambda_{k\alpha}\sum_{j=1}^{q} w_{jk\alpha}\cdot|\beta_{jk\alpha}| + \frac{\gamma_{k\alpha}}{2}\sum_{j=1}^{q}\beta_{jk\alpha}^2, \qquad (1)$$

where $K(m_i - m_\alpha|h_k)$ is a Gaussian kernel function defined by

$$K(m_i - m_\alpha|h_k) = \exp\left\{-\frac{1}{h_k}(m_i - m_\alpha)^2\right\},$$

and $\lambda_{k\alpha}$ and $\gamma_{k\alpha}$ are hyperparameters that control the L_1 (lasso [68]) and L_2 (ridge [69]) penalties, respectively. In addition, $w_{jk\alpha}$ is an importance weight for $\beta_{jk\alpha}$, and h_k is the bandwidth of the Gaussian kernel. The kernel function $K(m_i - m_\alpha|h_k)$ defines the neighborhood around the α-th sample in terms of $\boldsymbol{M}$; a large value of $K(m_i - m_\alpha|h_k)$ means that the i-th sample is in the neighborhood of the α-th sample. By fixing $\lambda_{k\alpha}$, $\gamma_{k\alpha}$, $w_{jk\alpha}$, and h_k, we obtain the estimates

$$\{\hat\beta_{1k\alpha},\ldots,\hat\beta_{qk\alpha}\} = \arg\min_{\beta_{jk\alpha}} L_k(\beta_{1k\alpha},\ldots,\beta_{qk\alpha}).$$

This parameter estimation method is a weighted version of the elastic net [22]. The L_1 penalty zeroes some coefficients [68], which produces a sparse network structure. In contrast, the L_2 penalty stabilizes the solution by a grouping effect that promotes the collective inclusion or exclusion of highly correlated variables in the model [22]. The importance weights $w_{jk\alpha}$ allow tuning parameters to take on different values for different coefficients $\beta_{jk\alpha}$. For example, if $w_{jk\alpha}$ has a large value, then an estimator $\hat\beta_{jk\alpha}$ tends to be zero. In contrast, if $w_{jk\alpha}$ has a small value that is nearly equal to zero, $\hat\beta_{jk\alpha}$ tends to be non-zero. These weights create a sparser network structure than the lasso and elastic net methods. The parameters $\beta_{jk\alpha}$ were estimated by using a recursive procedure, and the weights $w_{jk\alpha}$ were updated by $w_{jk\alpha} = 1/(\tilde\beta_{jk\alpha} + \xi)$ [70], where $\tilde\beta_{jk\alpha}$ is the estimate from the previous step and $\xi = 10^{-5}$ to avoid dividing by zero. Then, the modulator-dependent networks for n samples can be derived from the estimates of $\hat\beta_{jk\alpha}$ ($j = 1,\ldots,q$, $k = 1,\ldots,p$, and $\alpha = 1,\ldots,n$).

For convenience of subsequent explanations, we introduce the following notations:

$$\boldsymbol{t}_{k\alpha}(h_k) = \begin{pmatrix} \kappa_{1\alpha}(h_k)\cdot t_{1k} \\ \vdots \\ \kappa_{n\alpha}(h_k)\cdot t_{nk} \end{pmatrix}, and$$

$$\boldsymbol{R}_\alpha(h_k) = \begin{pmatrix} \kappa_{1\alpha}(h_k)\cdot r_{11} & \cdots & \kappa_{1\alpha}(h_k)\cdot r_{1q} \\ \vdots & \ddots & \vdots \\ \kappa_{n\alpha}(h_k)\cdot r_{n1} & \cdots & \kappa_{n\alpha}(h_k)\cdot r_{nq} \end{pmatrix},$$

where $\kappa_{i\alpha}(h_k) = \sqrt{K(m_i - m_\alpha|h_k)}$.

In these expressions, $\boldsymbol{t}_{k\alpha}(h_k)$ and $\boldsymbol{R}_\alpha(h_k)$ were normalized so that the means and variances for $\boldsymbol{t}_{k\alpha}(h_k)$ and each column of $\boldsymbol{R}_\alpha(h_k)$ were 0 and 1, respectively. As a result, the intercept $\beta_{0k\alpha}$ was not included in the loss function (1). For fixed h_k, the loss function (1) can be minimized by using a kernel-based weighted version of the recursive elastic net [70]. The tuning parameters $\lambda_{k\alpha}$ and $\gamma_{k\alpha}$ were selected by minimizing a modified version of the bias-corrected weighted Akaike information criterion (AIC) [71]:

$$\mathrm{mWAICc}_{k\alpha} = (n_\alpha(h_k)+1)\cdot\log(2\pi\hat\sigma_{k\alpha}^2) + \frac{2n_\alpha(h_k)(\hat{\mathrm{df}}_{k\alpha}+1)}{n_\alpha(h_k) - \hat{\mathrm{df}}_{k\alpha} - 2},$$

where $n_\alpha(h_k) = \sum_{i=1}^{n}\kappa_{i\alpha}(h_k)$, and $\hat\sigma_{k\alpha}^2$ is estimated by

$$\hat\sigma_{k\alpha}^2 = \frac{1}{n_\alpha(h_k)}\|\boldsymbol{t}_{k\alpha}(h_k) - \boldsymbol{R}_\alpha(h_k)\hat\beta_{k\alpha}\|_2^2,$$

with $\hat\beta_{k\alpha} = (\hat\beta_{1k\alpha},\ldots,\hat\beta_{qk\alpha})'$. In addition, $\hat{\mathrm{df}}_{k\alpha}$ is the unbiased estimate of the degrees of freedom given by

$$\hat{\mathrm{df}}_{k\alpha} = tr\left[(\tilde{\boldsymbol{R}}(h_k)'\tilde{\boldsymbol{R}}(h_k) + \gamma_{k\alpha}\boldsymbol{I})^{-1}\tilde{\boldsymbol{R}}(h_k)'\tilde{\boldsymbol{R}}(h_k)\right],$$

where $\boldsymbol{I}$ is the identify matrix and $\tilde{\boldsymbol{R}}(h_k)$ is the submatrix of $\boldsymbol{R}(h_k)$, which has columns that correspond to the nonzero coefficients, respectively.

The NetworkProfiler algorithm is shown below:

Algorithm: NetworkProfiler.

```
$\tilde w_{jk\alpha} \leftarrow 1$ $(j = 1,\ldots,q)$
iter $\leftarrow$ 1
for $\gamma_{k\alpha} = \gamma[r]$ $(r = 1,\ldots,G)$ do
    repeat
        Calculate $\hat\beta_{k\alpha}[l,r]$ and $\mathrm{mWAICc}_{k\alpha}[l,r]$ corresponding to $\lambda_{k\alpha} = \lambda_k[l]$ $(l = 1,\ldots,L)$.
        $z_r[\mathrm{iter}] \leftarrow \min\{\mathrm{mWAICc}_{k\alpha}(l,r); l = 1,\ldots,L\}$
        $l^* \leftarrow \arg\min_l\{\mathrm{mWAICc}_{k\alpha}(l,r); l = 1,\ldots,L\}$
        if $z_r[\mathrm{iter}] - z_r[\mathrm{iter}-1] > 0$ then
            Exit loop
        else
            $z^*[r] \leftarrow z_r[\mathrm{iter}]$
            $\tilde\beta_{k\alpha}[r] \leftarrow \hat\beta_{k\alpha}[l^*,r]$
            $\tilde w_{jk\alpha} \leftarrow 1/(|\tilde\beta_{jk\alpha}(r)| + \xi)$ $(j = 1,\ldots,q)$
            iter $\leftarrow$ iter + 1
        end if
    untill iter reaches to $M$.
end for
$r^* \leftarrow \arg\min_r\{z^*[r]; r = 1,\ldots,G\}$
Return the coefficient vector $\hat\beta_{k\alpha} = \tilde\beta_{k\alpha}[r^*]$.
```

The results from NetworkProfiler, which are the estimates of q coefficients $\hat\beta_{jk\alpha}$ $(j = 1,\ldots,q)$ for the k-th target gene of the α-th patient, depend on the values of h_k. We used cross-validation to select an optimal value of h_k and estimate $q\times n$ coefficients, $\beta_{1k1},\ldots,\beta_{qkn}$ by minimizing the cross-validation error:

$$\mathrm{CV}_k = \sum_{\alpha\in\mathbb{S}}(t_{\alpha k} - \sum_{j=0}^{q}\hat\beta_{jk\alpha}^{(-\alpha)}\cdot r_{\alpha j})^2, \qquad (2)$$

where $\mathbb{S}$ is a randomly selected set of samples and $\hat\beta_{1k\alpha}^{(-\alpha)},\ldots,\hat\beta_{qk\alpha}^{(-\alpha)}$ are estimated from the remaining samples by minimizing:

$$L_k^{-\alpha}(\beta_{1k\alpha},\ldots,\beta_{qk\alpha}|h_k)=\frac{1}{2}\sum_{i\notin\mathbb{S}}\{t_{ik}-\sum_{j=0}^{q}\beta_{jk\alpha}\cdot r_{ij}\}^2K(m_i-m_\alpha|h_k)$$

$$+\lambda_{k\alpha}\sum_{j=1}^{q}w_{jk\alpha}\cdot|\beta_{jk\alpha}|+\frac{\gamma_{k\alpha}}{2}\sum_{j=1}^{q}\beta_{jk\alpha}^2. \qquad (3)$$

The algorithm in NetworkProfiler for minimizing this loss function (3) is shown below:

Algorithm: Conditional optimization with cross-validation.

```
for $h_k = h_l$ ($l = 1,\ldots,H$) do
    for all $\alpha$ such that $\alpha \in \mathbb{S}$ do
        Calculate $\hat{\beta}_{1k\alpha}^{(-\alpha)}[h_l],\ldots,\hat{\beta}_{qk\alpha}^{(-\alpha)}[h_l]$ with NetworkProfiler.
    end for
    Calculate $\mathrm{CV}_k[h_l]$.
end for
$h_k^* \leftarrow \mathrm{argmin}_{h_l}\{\mathrm{CV}_k[h_l]; l = 1,\ldots,H\}$
for $\alpha = 1,\ldots,n$ do
    Calculate $\hat{\beta}_{1k\alpha}[h_k^*],\ldots,\hat{\beta}_{qk\alpha}[h_k^*]$ with NetworkProfiler.
end for
Return a sequence of the coefficient vectors $\hat{\beta}_{k1}(h_k^*),\ldots,\hat{\beta}_{kn}(h_k^*)$.
```

Subsequently, the modulator-dependent gene networks for n samples are determined from the coefficient vectors $\hat{\beta}_{k1}(\hat{h}_k)$, …, $\hat{\beta}_{kn}(\hat{h}_k)$ $(k = 1,\ldots,p)$ by applying the above algorithm for all $k = 1,\ldots,p$. The computational cost of this algorithm rapidly increases as the number of samples and genes increase. Thus, for computers that only have a single central processing unit (CPU), this algorithm is only practical for medium-sized networks with up to several genes. However, since this algorithm can be executed in parallel for every k, it can be run on a stand-alone workstation with multi-core CPUs and computer clusters. Figure S4 represents the histogram of computational times based on 12 core CPUs (Intel Xeon Processor E5450 (# of cores = 4, clock speed = 3.0GHz) × 3) for calculating 762 cancer cell line-specific gene networks from 13,508 × 762 gene expression data through 100,000 iterations when 100 target genes were randomly selected among 13,508 genes and the number of regulators was not restricted, i.e., 1732 regulators were used. The average computational time was about 9 days. In this situation, we can find putative master regulators of the focused target genes related with a modulator of interest. Of course, for calculating gene networks of 762 samples for a large number of target genes, a supercomputer is required. In this study, we used the Super Computer System at the Human Genome Center, Institute of Medical Science, University of Tokyo, Japan, to analyze 762 gene networks with 13,508 target genes.

Signature-based hidden modulator extraction

When the modulator was a variable that is difficult to observe, we used a signature-based hidden modulator extraction algorithm to estimate the value of the modulator for each sample. This algorithm takes seed genes that are related to the modulator and computes the underlying latent variable of the modulator by using principal components and extraction of expression modules (EEM) [7]. Let $\mathbb{M}$ be a gene set that is related to the modulator and let $\boldsymbol{X}_{\mathbb{M}}$ be an $n \times |\mathbb{M}|$ matrix of n expression levels of $\mathbb{M}$. Then, a linear model, which is a special case of the single factor model [72], relates $\mathbb{M}^*$, a subset of $\mathbb{M}$, to an underlying latent variable U as follows:

$$X_j = \alpha_{0j} + \alpha_{1j}U + \varepsilon'_j,\ j \in \mathbb{M}^* \subseteq \mathbb{M}, \qquad (4)$$

where X_j is the expression level of the j-th gene in $\mathbb{M}^*$, α_{0j} is the y-intercept, α_{1j} is a coefficient, and ε'_j is a noise term. We assumed that other genes that do not include $\mathbb{M}^*$ $(\{X_j; j \notin \mathbb{M}^*\})$ are independent of U.

The values of U for n samples, u_i $(i = 1,\ldots,n)$, can be estimated by the following procedure:

Algorithm: signature-based hidden modulator extraction.

1: For a given set $\mathbb{M}$, find a subset $\mathbb{M}^*$ based on the expression coherence with the EEM algorithm [7].

2: Given $\mathbb{M}^*$, singular value decomposition of the data matrix $\boldsymbol{X}_{\mathbb{M}^*}$ estimates u_i by the largest principal component.

3: Return the values u_i $(i = 1,\ldots,n)$.

In the first step, we estimate $\mathbb{M}^*$. In the second step, we assume that the noise terms ε'_j have Gaussian distributions with equal variances. As a result, the singular value decomposition generates maximum likelihood estimates of u_i for the single factor model [72].

Regulatory effect

To identify upstream regulators that had strong effects on the expression of a target gene of interest in the constructed modulator-dependent gene networks, we defined a measure, called the regulatory effect, of the effect of the j-th regulator on the k-th target gene in the α-th sample as

$$\mathrm{RE}_{jk\alpha} = \sum_{l \in \pi_{jk\alpha}} \hat{\beta}_l^{(j\to k)}(m_\alpha)\cdot r_{\alpha j}, \qquad (5)$$

where $\pi_{jk\alpha}$ is the set of all possible paths from R_j to T_k, and $\hat{\beta}_l^{(j\to k)}(m_\alpha)$ is the product of the estimated coefficients on the l-th path that includes $\pi_{jk\alpha}$. For example, given all the possible paths from R_1 to T_2 in the α-th sample (Figure S5), the set $\pi_{12\alpha}$ is

$$\pi_{12\alpha} = \{R_1 \to T_2, R_1 \to R_3 \to T_2, R_1 \to R_3 \to R_4 \to T_2\}, \qquad (6)$$

and the regulatory effect $\mathrm{RE}_{12\alpha}$ is

$$\mathrm{RE}_{12\alpha} = (\hat{\beta}_{12\alpha} + \hat{\beta}_{13\alpha}\cdot\hat{\beta}_{32\alpha} + \hat{\beta}_{13\alpha}\cdot\hat{\beta}_{34\alpha}\cdot\hat{\beta}_{42\alpha})\cdot r_{\alpha j}. \qquad (7)$$

In our analysis, the length of the paths from R_j to T_k is restricted to either 1 or 2.

To determine how the modulator affects the regulatory effect $\mathrm{RE}_{jk\alpha}$, we also defined the change in the regulatory effect of the j-th regulator on the k-th target as

$$\mathrm{REC}_{jk} = \max\{\mathrm{RE}_{jk\alpha}; \alpha = 1,\ldots,n\} - \min\{\mathrm{RE}_{jk\alpha}; \alpha = 1,\ldots,n\}. \qquad (8)$$

In addition to this definition, it is also possible to use percentiles instead of max and min to achieve more robust results. However, in our analysis, we used max and min to increase the power of the method. It should be noted that the change in the regulatory effect REC_{jk} does not explain the mode of action for the modulator with respect to the regulator-target relationship. File S5 (http://bonsai.hgc.jp/~shima/NetworkProfiler) is provided to determine the modulator mode of action by statistical test.

Gene set analysis of downstream genes for a regulator

To identify regulators that enhanced the functions of their targets, we calculated the statistical significance of the enrichment of targets for a given regulator in each sample. To test the enrichment, we use the degree of independence between the two properties:

$\mathcal{A}_{j\alpha}$:gene is in the list of targets for the j-th regulator in the $\alpha-$th sample

$\mathcal{B}_u$:gene is a member of the u-th priori set

Testing the association between the properties $\mathcal{A}_{j\alpha}$ and $\mathcal{B}_u$ corresponds to Fisher's exact test. The p-value calculated by this test, $\mathrm{P}_{ju\alpha}$, indicates the probability of observing at least the same amount of enrichment when downstream genes are randomly selected out of all genes. Thus, a very small p-value gives strong evidence for an association between $\mathcal{A}_{j\alpha}$ and $\mathcal{B}_u$ for the j-th regulator in the α-th sample. To correct for multiple hypotheses testing, Benjamini-Hochberg (BH)-corrected p-values (q-values) [73], $\mathrm{Q}_{ju\alpha}$, were calculated.

To determine how the modulator affects the functions of downstream genes for a regulator, we defined the enrichment score, ES_{ju}, as a change in the statistical significance of the enrichment of targets for the j-th regulator on the u-th function:

$$\mathrm{ES}_{ju} = \log(\max\{\mathrm{Q}_{ju\alpha};\alpha=1,\ldots,n\}/\min\{\mathrm{Q}_{ju\alpha};\alpha=1,\ldots,n\}). \quad (9)$$

Thus, a very large ES_{ju} indicates that the modulator causes a significant change of the enrichment of the targets for the j-th regulator on the u-th function.

To identify putative master regulators that control more functional gene sets than other regulators, we also calculated the total enrichment score, TES_j, by combining independent enrichment scores, $\mathrm{ES}_{j1},\ldots,\mathrm{ES}_{jU}$, where U is the number of functional gene sets:

$$\mathrm{TES}_j = 2\sum_{u=1}^{U} \mathrm{ES}_{ju}. \quad (10)$$

The total enrichment score is equivalent to the difference of the Fisher's statistic $-2\sum_{i=1}^{k}\log\,\mathrm{P}_k$ [74] which was used to combine independent tests obtained from k studies based on the p-values, $\mathrm{P}_1,\ldots,\mathrm{P}_k$. The Fisher's method is based on the fact that the statistic $-2\sum_{i=1}^{k}\log\,\mathrm{P}_i$ follows a chi-square distribution with $2k$ degrees of freedom under the global null hypothesis that all null hypotheses are true. A small integral p-value for the hypothesis indicates that the j-th regulator controlled at least one or more functional gene sets during the change of the modulator.

Supporting Information

Figure S1 Quantitative real-time RT-PCR analysis of KLF5 in siKLF5-treated A549 cells.
(PDF)

Figure S2 Expression profiles of miR-100 in order of ascending the EMT-related modulator values.
(PDF)

Figure S3 miR-100-induced changes in biologic characteristics in NCI-H1437 and NCI-H727 NSCLC cell lines. (a) Representative phase contrast microscopic images showing negligible changes in morphology by miR-100 introduction in both NSCLC cells lines. NC#2, negative control. (b) Motility assay showing increased migration by introduction of miR-100 in both NSCLC cell lines. *, $P<0.05$.
(PDF)

Figure S4 Histogram of computational times for inferring cancer cell line-specific gene networks running on 12 core CPUs. The 762 cancer cell line-specific gene networks related with the EMT were calculated from 13,508 × 762 gene expression data when 100 target genes were randomly selected among 13,508 genes and the number of regulators was not restricted, i.e., 1,732 regulators were used. The comptational times were based on 12 core CPUs (Intel Xeon Processor E5450 (# of cores $=4$, clock speed $=3.0$ GHz$)\times 3$). The histogram was calculated by 100,000 iterations.
(PDF)

Figure S5 Example of paths among four genes, R_1, T_2, R_3 , and R_4.
(PDF)

Table S1 List of candidate regulators mapped to 1183 transcription factors and 47 nuclear receptors.
(XLS)

Table S2 List of candidate regulators mapped to 502 human microRNAs.
(XLS)

Table S3 List of coherent genes (p-value$<10^{-5}$) related to EMT calculated by extraction of expression module (EEM).
(XLS)

Table S4 EMT-related modulator values of 762 cancer cell lines calculated by signature-based hidden modulator extraction.
(XLS)

Table S5 List of 370 putative master regulators of E-cadherin during the EMT which were estimated by NetworkProfiler.
(XLS)

Table S6 List of 627 putative master regulators of E-cadherin which were estimated by a structual equation model (SEM) with the elastic net.
(XLS)

Table S7 Regulator function matrix between 1732 regulators and 5 functions. The row and column indicate regulator and functional gene set, respectively. The (i,j)-th element represents the change during the EMT in the statistical significance (-$\log_{10}$(q-value)) for the enrichment of target genes of the i-th regulator on the j-th function. The last column indicate the integral q-value of each row regulator which were used to determine which regulator strongly affected the functional gene sets.
(XLS)

Table S8 List of 17 putative master regulators (integral q-value$<10^{-10}$) which correlated at least one or more EMT-related functions and were known to be downstream targets of TGFB1 with published evidence from Ingenuity Knowledge Base (http://www.ingenuity.com).
(XLS)

Table S9 List of the changes in the regulatory effects from 1732 regulators to E-cadherin and vimentin during the EMT.
(XLS)

Acknowledgments

The supercomputing resource was provided by Human Genome Center (University of Tokyo).

Author Contributions

Conceived and designed the experiments: TT. Performed the experiments: YS YH. Analyzed the data: TS AN. Wrote the paper: TS. Organized the project: SM. Provided statistical expertise: SI RY. Provided computational expertize: AN MN. Provided experimental expertise: TT. Provided manuscript review: SI AN RY TT.

References

1. Wang E (2010) Cancer systems biology CRC Press.
2. Schisky RL (2010) Personalized medicine in oncology: the future is now. Nat Rev Drug Discov 9(5): 363–6.
3. Gonzalez-Angulo AM, Hennessy BT, Mills GB (2010) Future of personalized medicine in oncology: a systems biology approach. J Clin Oncol 28(16): 2777–83.
4. Bansal M, Belcastro V, Ambesi-Impiombato A, di Bernardo D (2007) How to infer gene networks from expression profiles. Mol Syst Biol 3: 78.
5. Thiery JP, Acloque H, Huang RY, Nieto MA (2009) Epithelial-mesenchymal transitions in development and disease. Cell 139(5): 871–90.
6. Subramanian A, Tamayo P, Mootha VK, Mukherjee S, Ebert BL, et al. (2005) Gene set enrichment analysis: a knowledge-based approach for interpreting genome-wide expression profiles. Proc Natl Acad Sci U S A 102(43): 15545–50.
7. Niida A, Smith AD, Imoto S, Aburatani H, Zhang MQ, et al. (2009) Gene set-based module discovery in the breast cancer transcriptome. BMC Bioinformatics 10: 71.
8. Gregory PA, Bert AG, Paterson EL, Barry SC, Tsykin A, et al. (2008) The miR-200 family and miR-205 regulate epithelial to mesenchymal transition by targeting ZEB1 and SIP1. Nat Cell Biol 10(5): 593–601.
9. Comijn J, Berx G, Vermassen P, Verschueren K, van Grunsven L, et al. (2001) The two-handed E box binding zinc finger protein SIP1 downregulates E-cadherin and induces invasion. Mol Cell 7(6): 1267–78.
10. Yori JL, Johnson E, Zhou G, Jain MK, Keri RA (2010) Kruppel-like factor 4 inhibits epithelial-tomesenchymal transition through regulation of E-cadherin gene expression. J Biol Chem 285(22): 16854–63.
11. Song Y, Washington MK, Crawford HC (2010) Loss of FOXA1/2 is essential for the epithelialto-mesenchymal transition in pancreatic cancer. Cancer Res 70(5): 2115–25.
12. Sobrado VR, Moreno-Bueno G, Cubillo E, Holt LJ, Nieto MA, et al. (2009) The class I bHLH factors E2-2A and E2-2B regulate EMT. J Cell Sci 122(Pt 7): 1014–24.
13. Kato M, Zhang J, Wang M, Lanting L, Yuan H, et al. (2007) MicroRNA-192 in diabetic kidney glomeruli and its function in TGF-beta-induced collagen expression via inhibition of E-box repressors. Proc Natl Acad Sci U S A 104(9): 3432–7.
14. Wang B, Herman-Edelstein M, Koh P, Burns W, Jandeleit-Dahm K, et al. (2010) E-cadherin expression is regulated by miR-192/215 by a mechanism that is independent of the profibrotic effects of transforming growth factor-beta. Diabetes 59(7): 1794–802.
15. Eger A, Aigner K, Sonderegger S, Dampier B, Oehler S, et al. (2005) DeltaEF1 is a transcriptional repressor of E-cadherin and regulates epithelial plasticity in breast cancer cells. Oncogene 24(14): 2375–85.
16. Hajra KM, Chen DY, Fearon ER (2002) The SLUG zinc-finger protein represses E-cadherin in breast cancer. Cancer Res 62(6): 1613–8.
17. Yang J, Mani SA, Donaher JL, Ramaswamy S, Itzykson RA, et al. (2004) Twist, a master regulator of morphogenesis, plays an essential role in tumor metastasis. Cell 117(7): 927–39.
18. Perez-Moreno MA, Locascio A, Rodrigo I, Dhondt G, Portillo F, et al. (2001) A new role for E12/E47 in the repression of E-cadherin expression and epithelial-mesenchymal transitions. J Biol Chem 276(29): 27424–31.
19. Almeida MS, Bray SJ (2005) Regulation of post-embryonic neuroblasts by Drosophila Grainyhead. Mech Dev 122(12): 1282–93.
20. Cowger JJ, Zhao Q, Isovic M, Torchia J (2007) Biochemical characterization of the zinc-finger protein 217 transcriptional repressor complex: identification of a ZNF217 consensus recognition sequence. Oncogene 26(23): 3378–86.
21. Yang Y, Goldstein BG, Chao HH, Katz JP (2005) KLF4 and KLF5 regulate proliferation, apoptosis and invasion in esophageal cancer cells. Cancer Biol Ther 4(11): 1216–21.
22. Zou H, Hastie T (2005) Regularization and variable selection via the elastic net. J Roy Statist Soc Ser B 67: 301–20.
23. Bracken CP, Gregory PA, Kolesnikoff N, Bert AG, Wang J, et al. (2008) A double-negative feedback loop between ZEB1-SIP1 and the microRNA-200 family regulates epithelial-mesenchymal transition. Cancer Res 68(19): 7846–54.
24. Willis BC, Borok Z (2007) TGF-beta-induced EMT: mechanisms and implications for fibrotic lung disease. Am J Physiol Lung Cell Mol Physiol 293(3): L525–34.
25. Chen H, Zhu G, Li Y, Padia RN, Dong Z, et al. (2009) Extracellular signal-regulated kinase signaling pathway regulates breast cancer cell migration by maintaining slug expression. Cancer Res 69(24): 9228–35.
26. Adiseshaiah P, Lindner DJ, Kalvakolanu DV, Reddy SP (2007) FRA-1 proto-oncogene induces lung epithelial cell invasion and anchorage-independent growth in vitro, but is insufficient to promote tumor growth in vivo. Cancer Res 67(13): 6204–11.
27. Cowden Dahl KD, Robertson SE, Weaver VM, Simon MC (2005) Hypoxia-inducible Factor Regulates alphavbeta3 Integrin Cell Surface Expression. Mol Biol Cell 16(4): 1901–12.
28. Imtiyaz HZ, Williams EP, Hickey MM, Patel SA, Durham AC, et al. (2010) Hypoxia-inducible factor 2alpha regulates macrophage function in mouse models of acute and tumor inflammation. J Clin Invest 120(8): 2699–714.
29. Yang Y, Tetreault MP, Yermolina YA, Goldstein BG, Katz JP (2008) Kruppel-like Factor 5Controls Keratinocyte Migration via the Integrin-linked Kinase. J Biol Chem 283(27): 18812–20.
30. Marlowe JL, Puga A (2005) Aryl hydrocarbon receptor, cell cycle regulation, toxicity, and tumorigenesis. J Cell Biochem 96(6): 1174–84.
31. Nakagawa H, Liyanarachchi S, Davuluri RV, Auer H, Martin EW, et al. (2004) Role of cancerassociated stromal fibroblasts in metastatic colon cancer to the liver and their expression profiles. Oncogene 23(44): 7366–77.
32. Malin D, Kim IM, Boetticher E, Kalin TV, Ramakrishna S, et al. (2007) Forkhead box f1 is essential for migration of mesenchymal cells and directly induces integrin-beta3 expression. Mol Cell Biol 27(7): 2486–98.
33. Buchwalter G, Gross C, Wasylyk B (2005) The Ternary Complex Factor Net Regulates Cell Migration through Inhibition of PAI-1 Expression. Mol Cell Biol 25(24): 10853–62.
34. Hayes SA, Huang X, Kambhampati S, Platanias LC, Bergan RC (2003) p38 MAP kinase modulatesSmad-dependent changes in human prostate cell adhesion. Oncogene 22(31): 4841–50.
35. Matsuzaki K, Kitano C, Murata M, Sekimoto G, Yoshida K, et al. (2009) Smad2 and Smad3 phosphorylated at both linker and COOH-terminal regions transmit malignant TGF-beta signal in later stages of human colorectal cancer. Cancer Res 69(13): 5321–30.
36. Sekimoto G, Matsuzaki K, Yoshida K, Mori S, Murata M, et al. (2007) Reversible Smad-Dependent Signaling between Tumor Suppression and Oncogenesis. Cancer Res 67(11): 5090–6.
37. Sato M, Muragaki Y, Saika S, Roberts AB, Ooshima A (2003) Targeted disruption of TGFbeta1/Smad3 signaling protects against renal tubulointerstitial fibrosis induced by unilateral ureteral obstruction. J Clin Invest 112(10): 1486–94.
38. Chan SW, Lim CJ, Guo K, Ng CP, Lee I, et al. (2008) A role for TAZ in migration, invasion, and tumorigenesis of breast cancer cells. Cancer Res 68(8): 2592–8.
39. Sachdeva M, Mo YY (2010) MicroRNA-145 suppresses cell invasion and metastasis by directly targeting mucin 1. Cancer Res 70(1): 378–87.
40. Matsuya M, Sasaki H, Aoto H, Mitaka T, Nagura K, et al. (1998) Cell adhesion kinase beta forms a complex with a new member, Hic-5, of proteins localized at focal adhesions. J Biol Chem 273(2): 1003–14.
41. Lu X, Yan CH, Yuan M, Wei Y, Hu G, et al. (2010) In vivo dynamics and distinct functions of hypoxia in primary tumor growth and organotropic metastasis of breast cancer. Cancer Res 70(10): 3905–14.
42. Okuyama H, Krishnamachary B, Zhou YF, Nagasawa H, Bosch-Marce M, et al. (2006) Expressionof vascular endothelial growth factor receptor 1 in bone marrow-derived mesenchymal cells is dependent on hypoxia-inducible factor 1. J Biol Chem 281(22): 15554–63.
43. Kim KS, Sengupta S, Berk M, Kwak YG, Escobar PF, et al. (2006) Hypoxia Enhances Lysophosphatidic Acid Responsiveness in Ovarian Cancer Cells and Lysophosphatidic Acid Induces Ovarian Tumor Metastasis In vivo. Cancer Res 66(16): 7983–90.
44. Schedin PJ, Eckel-Mahan KL, McDaniel SM, Prescott JD, Brodsky KS, et al. (2004) ESX induces transformation and functional epithelial to mesenchymal transition in MCF-12A mammary epithelial cells. Oncogene 23(9): 1766–79.
45. Panda DK, Miao D, Lefebvre V, Hendy GN, Goltzman D (2001) The transcription factor SOX9 regulates cell cycle and differentiation genes in chondrocytic CFK2 cells. J Biol Chem 276(44): 41229–36.
46. Mori-Akiyama Y, Akiyama H, Rowitch DH, de Crombrugghe B (2003) Sox9 is required for determination of the chondrogenic cell lineage in the cranial neural crest. Proc Natl Acad Sci U S A 100(16): 9360–5.
47. Tomioka N, Osumi N, Sato Y, Inoue T, Nakamura S, et al. (2000) Neocortical origin and tangential migration of guidepost neurons in the lateral olfactory tract. J Neurosci 20(15): 5802–12.
48. Jean C, Blanc A, Prade-Houdellier N, Ysebaert L, Hernandez-Pigeon H, et al. (2009) Epidermal growth factor receptor/beta-catenin/T-cell factor 4/matrix metalloproteinase 1: a new pathway for regulating keratinocyte invasiveness after UVA irradiation. Cancer Res 69(8): 3291–9.
49. Minami T, Miura M, AirdWC, Kodama T (2006) Thrombin-induced Autoinhibitory Factor, Down Syndrome Critical Region-1, Attenuates NFAT-dependent Vascular Cell Adhesion Molecule-1 Expression and Inflammation in the Endothelium. J Biol Chem 281(29): 20503–20.

50. Huang S, Pettaway CA, Uehara H, Bucana CD, Fidler IJ (2001) Blockade of NF-kappaB activity in human prostate cancer cells is associated with suppression of angiogenesis, invasion, and metastasis. Oncogene 20(31): 4188–97.
51. Shair KH, Schnegg CI, Raab-Traub N (2008) EBV Latent Membrane Protein 1 Effects on Plakoglobin, Cell Growth, and Migration. Cancer Res 68(17): 6997–7005.
52. Gakidis MA, Cullere X, Olson T, Wilsbacher JL, Zhang B, et al. (2004) Vav GEFs are required for beta2 integrin-dependent functions of neutrophils. J Cell Biol 166(2): 273–82.
53. Schymeinsky J, Sindrilaru A, Frommhold D, Sperandio M, Gerstl R, et al. (2006) The Vav binding site of the non-receptor tyrosine kinase Syk at Tyr 348 is critical for beta2 integrin (CD11/CD18)- mediated neutrophil migration. Blood 108(12): 3919–27.
54. Hong IK, Jin YJ, Byun HJ, Jeoung DI, Kim YM, et al. (2006) Homophilic Interactions of Tetraspanin CD151 Up-regulate Motility and Matrix Metalloproteinase-9 Expression of Human Melanoma Cells through Adhesion-dependent c-Jun Activation Signaling Pathways. J Biol Chem 281(34): 24279–92.
55. Janulis M, Silberman S, Ambegaokar A, Gutkind JS, Schultz RM (1999) Role of mitogen-activated protein kinases and c-Jun/AP-1 trans-activating activity in the regulation of protease mRNAs and the malignant phenotype in NIH 3T3 fibroblasts. J Biol Chem 274(2): 801–13.
56. Cai C, Hsieh CL, Omwancha J, Zheng Z, Chen SY, et al. (2007) ETV1 Is a Novel Androgen Receptor-Regulated Gene that Mediates Prostate Cancer Cell Invasion. Mol Endocrinol 21(8): 1835–46.
57. Bauer K, Kratzer M, Otte M, de Quintana KL, Hagmann J, et al. (2000) Human CLP36, a PDZdomain and LIM-domain protein, binds to alpha-actinin-1 and associates with actin filaments and stress fibers in activated platelets and endothelial cells. Blood 96(13): 4236–45.
58. Zent CS, Mathieu C, Claxton DF, Zhang DE, Tenen DG, et al. (1996) The chimeric genes AML1/MDS1 and AML1/EAP inhibit AML1B activation at the CSF1R promoter, but only AML1/MDS1 has tumor-promoter properties. Proc Natl Acad Sci U S A 93(3): 1044–8.
59. Perry C, Sklan EH, Birikh K, Shapira M, Trejo L, et al. (2002) Complex regulation of acetylcholinesterase gene expression in human brain tumors. Oncogene 21(55): 8428–41.
60. Zhang X, Milton CC, Humbert PO, Harvey KF (2009) Transcriptional output of the Salvador/ warts/hippo pathway is controlled in distinct fashions in Drosophila melanogaster and mammalian cell lines. Cancer Res 69(15): 6033–41.
61. Aung CS, Hill MM, Bastiani M, Parton RG, Parat MO (2010) PTRF-cavin-1 expression decreases the migration of PC3 prostate cancer cells: role of matrix metalloprotease 9. Eur J Cell Biol, 2010 Aug 21. [Epub ahead of print].
62. Hurst DR, Edmonds MD, Scott GK, Benz CC, Vaidya KS, et al. (2009) Breast cancer metastasis suppressor 1 up-regulates miR-146, which suppresses breast cancer metastasis. Cancer Res 69(4): 1279–83.
63. Cordes KR, Sheehy NT, White MP, Berry EC, Morton SU, et al. (2009) miR-145 and miR-143 regulate smooth muscle cell fate and plasticity. Nature 460(7256): 705–10.
64. Kasai H, Allen JT, Mason RM, Kamimura T, Zhang Z (2005) TGF-β1 induces human alveolar epithelial to mesenchymal cell transition (EMT). Respir Res 6: 56.
65. Taguchi A, Yanagisawa K, Tanaka M, Cao K, Matsuyama Y, et al. (2008) Identification of hypoxiainducible factor-1 alpha as a novel target for miR-17-92 microRNA cluster. Cancer Res 68(14): 5540–5.
66. Kozaki K, Miyaishi O, Tsukamoto T, Tatematsu Y, Hida T, et al. (2000) Establishment and characterization of a human lung cancer cell line NCI-H460-LNM35 with consistent lymphogenous metastasis via both subcutaneous and orthotopic propagation. Cancer Res 60(9): 2535–40.
67. Tokumaru S, Suzuki M, Yamada H, Nagino M, Takahashi T (2008) let-7 regulates Dicer expression and constitutes a negative feedback loop. Carcinogenesis 29(11): 2073–7.
68. Tibshirani R (1996) Regression shrinkage and selection via the lasso. J Royal Statist Soc B 58(1): 267–88.
69. Hoerl AE, Kennard R (1970) Ridge regression: biased estimation for nonorthogonal problems. Technometrics 12: 55–67.
70. Shimamura T, Imoto S, Yamaguchi R, Fujita A, Nagasaki M, et al. (2009) Recursive regularization for inferring gene networks from time-course gene expression profiles. BMC Syst Biol 3: 41.
71. Shimamura T, Imoto S, Yamaguchi R, Nagasaki M, Miyano S (2010) Inferring dynamic gene networks under varying conditions for transcriptomic network comparison. Bioinformatics 26(8): 1064–72.
72. Mardia K, Kent J, Bibby J (1979) Multivariate Analysis Academic Press.
73. Benjamini Y, Hochberg Y (1995) Controlling the false discovery rate: a practical and powerful approach to multiple testing. J Roy Statist Soc Ser B 57(1): 289–300.
74. Hartung J, Knapp G, Sinha BK (2008) Statistical meta-analysis with applications. Wiley.